The Aguablanca Ni–(Cu) sulfide deposit, SW Spain: geologic and geochemical controls and the relationship with a midcrustal layered mafic complex

Fernando Tornos · Carmen Galindo · César Casquet · Luis Rodríguez Pevida · César Martínez · Enrique Martínez · Francisco Velasco · Alexander Iriondo

Abstract The Aguablanca Ni–(Cu) sulfide deposit is hosted by a breccia pipe within a gabbro–diorite pluton. The deposit probably formed due to the disruption of a partially crystallized layered mafic complex at about 12–19 km depth and the subsequent emplacement of melts and breccias at shallow levels (<2 km). The ore-hosting breccias are interpreted as fragments of an ultramafic cumulate, which were transported to the near surface along with a molten sulfide melt. Phlogopite Ar–Ar ages are 341–332 Ma in the breccia pipe, and 338–334 Ma in the layered mafic complex, and are similar to recently reported U–Pb ages of the host Aguablanca Stock and other nearby calc-alkaline metaluminous intrusions (ca. 350–330 Ma). Ore deposition resulted from the combination of two critical factors, the emplacement of a layered mafic complex deep in the continental crust and the development of small dilational structures along transcrustal strike-slip faults that triggered the forceful intrusion of magmas to shallow levels. The emplacement of basaltic magmas in the lower middle crust was accompanied by major interaction with the host rocks, immiscibility of a sulfide melt, and the formation of a magma chamber with ultramafic cumulates and sulfide melt at the bottom and a vertically zoned mafic to intermediate magmas above. Dismembered bodies of mafic/ultramafic rocks thought to be parts of the complex crop out about 50 km southwest of the deposit in a tectonically uplifted block (Cortegana Igneous Complex, Aracena Massif). Reactivation of Variscan structures that merged at the depth of the mafic complex led to sequential extraction of melts, cumulates, and sulfide magma. Litho-geochemistry and Sr and Nd isotope data of the Aguablanca Stock reflect the mixing from two distinct reservoirs, i.e., an evolved siliciclastic middle-upper continental crust and a primitive tholeiitic melt. Crustal contamination in the deep magma chamber was so intense that orthopyroxene replaced olivine as the main mineral phase controlling the

early fractional crystallization of the melt. Geochemical evidence includes enrichment in SiO_2 and incompatible elements, and Sr and Nd isotope compositions ($^{87}Sr/^{86}Sr_i$ 0.708–0.710; $^{143}Nd/^{144}Nd_i$ 0.512–0.513). However, rocks of the Cortegana Igneous Complex have low initial $^{87}Sr/^{86}Sr$ and high initial $^{143}Nd/^{144}Nd$ values suggesting contamination by lower crustal rocks. Comparison of the geochemical and geological features of igneous rocks in the Aguablanca deposit and the Cortegana Igneous Complex indicates that, although probably part of the same magmatic system, they are rather different and the rocks of the Cortegana Igneous Complex were not the direct source of the Aguablanca deposit. Crust–magma interaction was a complex process, and the generation of orebodies was controlled by local but highly variable factors. The model for the formation of the Aguablanca deposit presented in this study implies that dense sulfide melts can effectively travel long distances through the continental crust and that dilational zones within compressional belts can effectively focus such melt transport into shallow environments.

Keywords Nickel · Magmatic sulfide deposits · Sulfide immiscibility · Aguablanca · Spain

Introduction

Most magmatic Ni–Cu deposits occur in greenstone belts, stable cratons, or rifted intraplate areas and are hosted by Mg-rich igneous rocks such as komatiite, picrite, anorthosite, or basalt-gabbro. Orebodies are located within stratiform magmatic complexes, sills, or lava flows or occur as subvertical bodies in the underlying feeder zones (Naldrett 1999). Only a few deposits, usually subeconomic, have been described in orogenic settings (see Naldrett 1989, 1999, 2004 for reviews). Thus, active continental margins have been considered as zones of minor interest for nickel exploration. This is probably the reason why the subouteropping deposit of Aguablanca was not discovered until 1993 when a regional stream geochemical survey detected a major Cu–Au anomaly within a gossan with only a few ancient trenches. Further drilling by Rio Tinto Minera and PRESUR led to the definition of an orebody that was acquired by Rio Narcea Recursos SA in 2001. Estimated proven and probable reserves are 15.7 Mt grading 0.66% Ni, 0.46% Cu, and 0.47 g/t PGE. Total ore mined in 2005 was 997,000 t with the production of 5,381 t of nickel and 4,888 t of copper. The deposit has been mined in an open pit since 2004, and there is no indication that the grade diminishes with depth. Underground mining is expected to start in early 2007 (http://www.rionarcea.com).

The orebody is hosted by the intermediate to mafic Aguablanca Stock, which is one of a number of metaluminous Variscan intrusions in SW Iberia (Fig. 1). The surrounding area contains different types of ore deposits and showings, including IOCG (Iron oxide–copper–gold) mineralization, iron-rich skarns, and Cu–(Au–Bi) veins (Tornos et al. 2004).

The immediate area near the orebody has been the subject of major research. The plutonic and the sedimentary host rocks were described by Velasco (1976), Casquet (1980, 1982), Casquet and Velasco (1978), Eguíluz et al. (1989), and Bateman et al. (1992, 1994). After the discovery of the deposit, several studies have been published, mainly dedicated to the mineralogy of the ore (Lunar et al. 1997; Bomati et al. 1999; Ortega et al. 1999–2002, 2004; Martín Estévez et al. 2000; Piña et al. 2005), the nature of the fragments in the breccia (Piña et al. 2004), and the geology, the geochemistry, and the origin of the deposit (Casquet et al. 1999, 2001; Tornos et al. 1999– 2002a). The latter contributions have shown that this deposit is remarkable in that it is the first case of a significant synorogenic magmatic Ni–(Cu) deposit related to calc-alkaline plutonism recorded to date. We in this study attempt to summarize our current geological and geochemical understanding of the Aguablanca deposit and its host rocks, placing the formation of the orebody into the regional framework of transpressional deformation during Variscan times and proposing relationships with sills emplaced deep into the crust. The comparison with an outcropping dismembered part of one of these deep sills (Cortegana Igneous Complex) gives clues on the overall evolution of these systems.

General geologic context

The Aguablanca orebody is located in the northeastern zone of the Santa Olalla Plutonic Complex, within the southernmost part of the Ossa Morena Zone of the Variscan Belt of Iberia (Fig. 1). The Ossa Morena Zone underwent a complex geodynamic evolution (see Quesada et al. 1991; Eguíluz et al. 2000, and references therein for reviews) with a Neoproterozoic Cadomian basement reworked by the Variscan orogeny. The Cadomian orogeny resulted from the subduction and subsequent collision of the exotic Ossa Morena terrane with the autochthonous Iberian terrane in the Late Neoproterozoic to Early Cambrian while the Variscan orogeny resulted from the oblique collision of the South Portuguese terrane with the southern margin of the Iberian Massif in the Devonian to Early Carboniferous. The Ossa Morena Zone hosts a wide suite of igneous rocks related to the two orogenies and to an intermediate rift-related pulse of Cambrian–Ordovician age (Sanchez Carretero et al. 1990; Eguíluz et al. 2000; Galindo and Casquet 2004). Variscan plutonism is volumetrically dominant and consists of calc-alkaline metaluminous composite intrusions ranging in

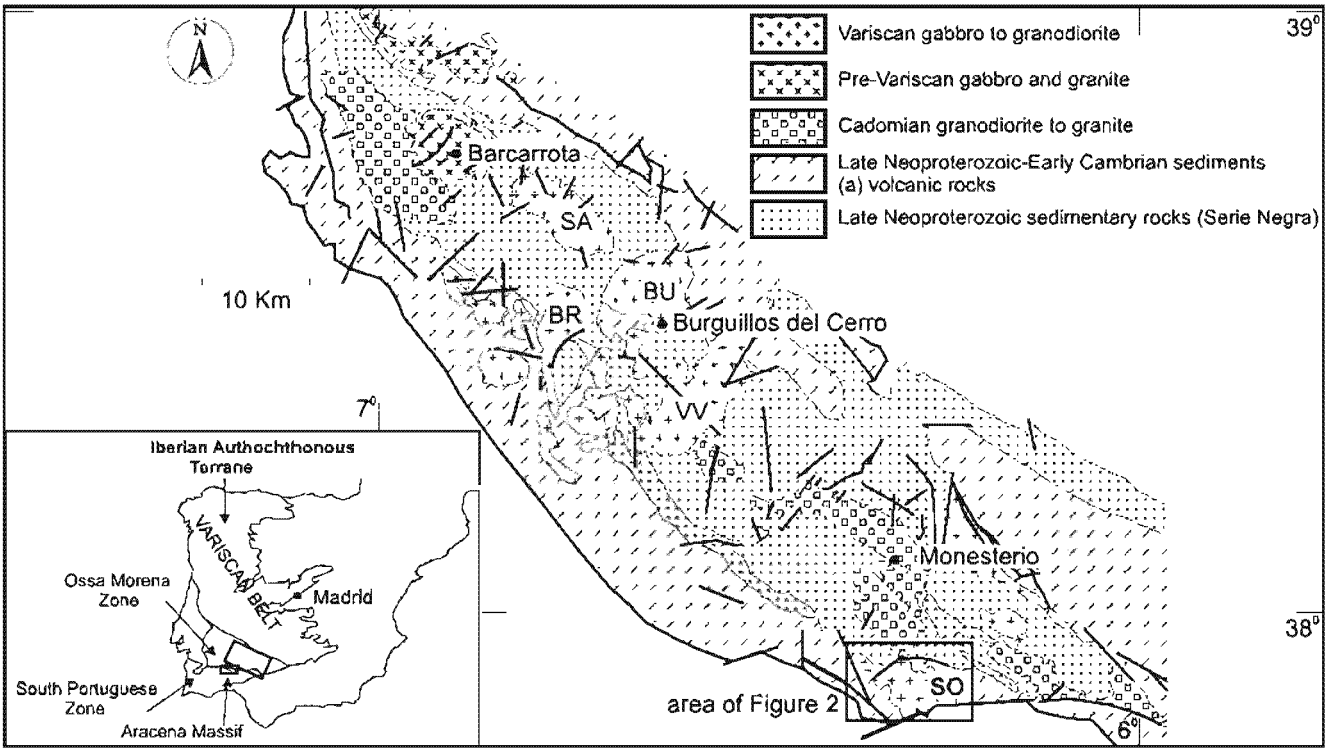

Fig. 1 Geology of the Central Part of the Ossa Morena Zone (Olivenza-Monesterio antiform) showing the major Variscan intrusions of the area. *BR* Brovales, *BU* Burguillos, *SA* Salvatierra, *SO* Santa Olalla Plutonic Complex, *VV* Valencia del Ventoso. The *inset* shows the location of the Ossa Morena Zone in the Variscan Belt of Iberia

composition from gabbro to granodiorite and minor peraluminous granite (Fig. 1).

During the Variscan deformation, the Ossa Morena Zone underwent thick-skinned deformation with the development of south-verging longitudinal fold-and-thrust zones that involved both the Cadomian basement and the Palaeozoic sedimentary cover. There are abundant contemporaneous and younger strike-slip faults. All these structures show evidence of formation in a transpressional setting in response to oblique subduction and played a major role in focusing magma ascent and pluton formation (Quesada et al. 1987; Tornos et al. 2005).

A major Variscan feature of the Ossa Morena Zone is the Olivenza-Monesterio antiform, where the Santa Olalla Plutonic Complex is located, of which the Aguablanca Stock and other intrusions are part (Fig. 1). Neoproterozoic rocks crop out in the core of this structure and consist of gray schist, quartzite, and graywacke with intercalated ortho-amphibolite (Serie Negra). Late Neoproterozoic to Middle Cambrian rocks unconformably overlie the Serie Negra and consist of syn-Cadomian calc-alkaline volcanic and subvolcanic rocks interbedded with graywacke, quartzite, limestone, and slate. Both sequences are overlain by a thick passive to rifted-margin sequence of limestone, siliciclastic metasedimentary rocks, and alkaline to subalkaline volcanic rocks of Early to Middle Cambrian age.

A second domain of interest in the Ossa Morena Zone is the Aracena Massif, which is a high-T low-P metamorphic belt located adjacent to the exotic South Portuguese terrane (Fig. 1). It includes a strained thick sequence of peraluminous gneiss with interbedded quartzite, pyroxene-bearing gneiss, ortho-amphibolite, limestone, and calc-silicate hornfels. This sequence is probably equivalent to the Late Neoproterozoic/Middle Cambrian sequence recognized elsewhere in the central and northern Ossa Morena Zone (Crespo 1991; Giese et al. 1994; Castro et al. 1999). The Aracena Massif hosts abundant bodies of mafic and ultramafic rocks remarkably similar to those of the Aguablanca Stock.

Recent seismic-reflection work has shown the existence of a 1-5-km-thick high-velocity zone at about 10 to 15 km depth throughout the Ossa Morena Zone where the large Variscan thrusts and faults are interpreted to be rooted (IRB, Iberian Reflective Body; Simancas et al. 2003; Carbonell et al. 2004). The more likely interpretation is that the reflector represents a large sill-like structure of mafic ultramafic rocks intruded during the Variscan times (Simancas et al. 2003). In detail, the IRB seems to be formed by several tens of lensoidal plutonic bodies separated by conductive graphite-rich shale, likely belonging to the Serie Negra (Pous et al. 2004; Tornos and Casquet 2005), and forming a layered magmatic complex similar in size to the Kunene or Bushveld complexes (Tornos et al. 2005). In this hypoth-

esis, the Aracena Massif represents an exhumed middle-lower crust section where dismembered parts of the magmatic complex crop out (Simancas et al. 2003; Tornos and Casquet 2005).

An alternative interpretation of the reflector has been proposed by Pous et al. (2004), relying on a hypothetical preferred orientation of graphite flake concentrations along the basal thrust. However, the coincidence with regional magnetometric data, the widespread low $^{207}Pb/^{206}Pb$ ratios of sulfides in the Ossa Morena Zone (Tornos and Chiaradia 2004), and the igneous geochemistry (Casquet et al. 2001) lend much support to the first hypothesis. Juvenile magmas probably intruded within a crustal decoupling zone, a major middle crust detachment, in response to oblique ridge collision at the Devonian–Carboniferous boundary (Tornos and Casquet 2005).

The Santa Olalla Plutonic Complex

The Santa Olalla Plutonic Complex is located in the southernmost Olivenza-Monesterio antiform and has intrusive contacts except in its southern part, where it ends abruptly against the Zufre Fault, which constitutes the limit between the Ossa Morena and South Portuguese Zones (Fig. 2).

The host rocks of the Santa Olalla Plutonic Complex underwent Variscan low-grade metamorphism before the plutonism (Casquet and Velasco 1978), and they belong to the Late Neoproterozoic to Middle Cambrian sequence. The Plutonic Complex reached its final emplacement level after the main thrusting and folding phase of the Variscan orogeny and produced an aureole of contact metamorphism about 2 km wide, which is only recognized south of the Cherneca Fault. Temperatures within the aureole attained values of the hypersthene hornfels facies (ca. 750°C) near the contact with the Aguablanca Stock, resulting in local partial melting. A depth of 1.7 to 3.5 km (0.5–1 kbar) was inferred for its emplacement from metamorphic mineral equilibria (Casquet 1980). Widespread garnet-pyroxene± magnetite skarn and minor magnesian skarn were formed by replacement of the marble and calc-silicate rocks before final emplacement of the Aguablanca Stock (Casquet and Velasco 1978; Casquet 1980).

The Santa Olalla Plutonic Complex includes the Santa Olalla Main Pluton, which is a large funnel-shaped intrusion with an apophysis to the NW, and the smaller Aguablanca Stock located in the northeastern part (Table 1, Fig. 2). The Main Pluton shows reverse compositional zoning with monzogranite and granodiorite in the center, tonalite in the middle, and amphibole-bearing quartz diorite in the edge (Velasco 1976; Casquet 1980; Casquet et al. 2001). U–Pb dating shows that the Santa Olalla Main Pluton and the Aguablanca Stock were broadly coeval. Ages of 332±3 Ma (Montero et al. 2000; U–Pb zircon, Kober method), 341±3 Ma (Romeo et al. 2004; U–Pb zircon, conventional), and 347±3.4 Ma (Spiering et al. 2005; U–Pb zircon, SHRIMP) are recorded for the Santa Olalla Main Pluton. The Aguablanca Stock, in turn, has yielded absolute ages of 338.6±0.8 Ma (Romeo et al. 2004) and 344±1.1 Ma (Spiering et al. 2005). With the exception of the 332±3.4 Ma value, the age sets for the two plutons are quite similar, although those of Spiering et al. (2005) are older by some 5 Ma. Geochemically and chronologically, the Santa Olalla Plutonic Complex is equivalent to other nearby intrusions such as Burguillos (336±1.6 to 338±1.3 Ma, Dallmeyer et al. 1995; 338±1.5 Ma, Casquet et al. 1998) and Brovales (340±7 Ma, Montero et al. 2000) (Fig. 1).

The Aguablanca Stock

The Aguablanca Stock is a small (ca. 10 km^2) and highly heterogeneous intrusion. The outer contacts are both concordant and discordant, and the internal architecture of the stock is interpreted as a half bell jar (Tornos et al. 2001). Moreover, detailed mapping suggests that the roof of the intrusion is close to the present erosion level as evidenced by the presence of roof pendants of skarnified marble and calc-silicate hornfels.

The intrusion consists of a dominant unit of medium-grained hornblende-biotite diorite and quartz diorite (Diorite Unit; Table 2, Fig. 3). These rocks are similar to the quartz diorite that forms the outer ring of the Santa Olalla Main Pluton (Casquet 1980). They have an inequigranular subeuhedral texture, locally subophitic, and consist of 2 to 3-mm-sized crystals of weakly zoned plagioclase of intermediate composition ($an_{46–51}$), diopside–augite, actinolitic hornblende, and biotite–phlogopite (Mg/Fe=2.3; Casquet 1980). Accessory minerals include quartz and trace amounts of apatite, pyrrhotite, and zircon.

The Gabbronorite Unit crops out in the northern part of the Aguablanca Stock. It consists for the most part of medium-grained massive gabbronorite with lesser amounts of pyroxene gabbro and norite in an approximate 2:1:1 ratio. A 10-m interval of faint layering resulting from modal and textural changes defined by alternating plagioclase- and mafic-rich centimeter-sized layers can be observed. Subhorizontal veins of pegmatitic gabbro and scapolite (Cl-rich meionite)-hedenbergite are locally present. The contact with the Diorite Unit is apparently gradational. At the contact with the host metasedimentary rocks, there is a discontinuous and up to 5- to 6-m-thick margin of fine-grained, phlogopite-rich gabbro (Contact Gabbro; Table 2).

Pyroxene occurs as unzoned crystals of between 0.5 and 3 mm, locally exhibiting a glomero-porphyritic disposition.

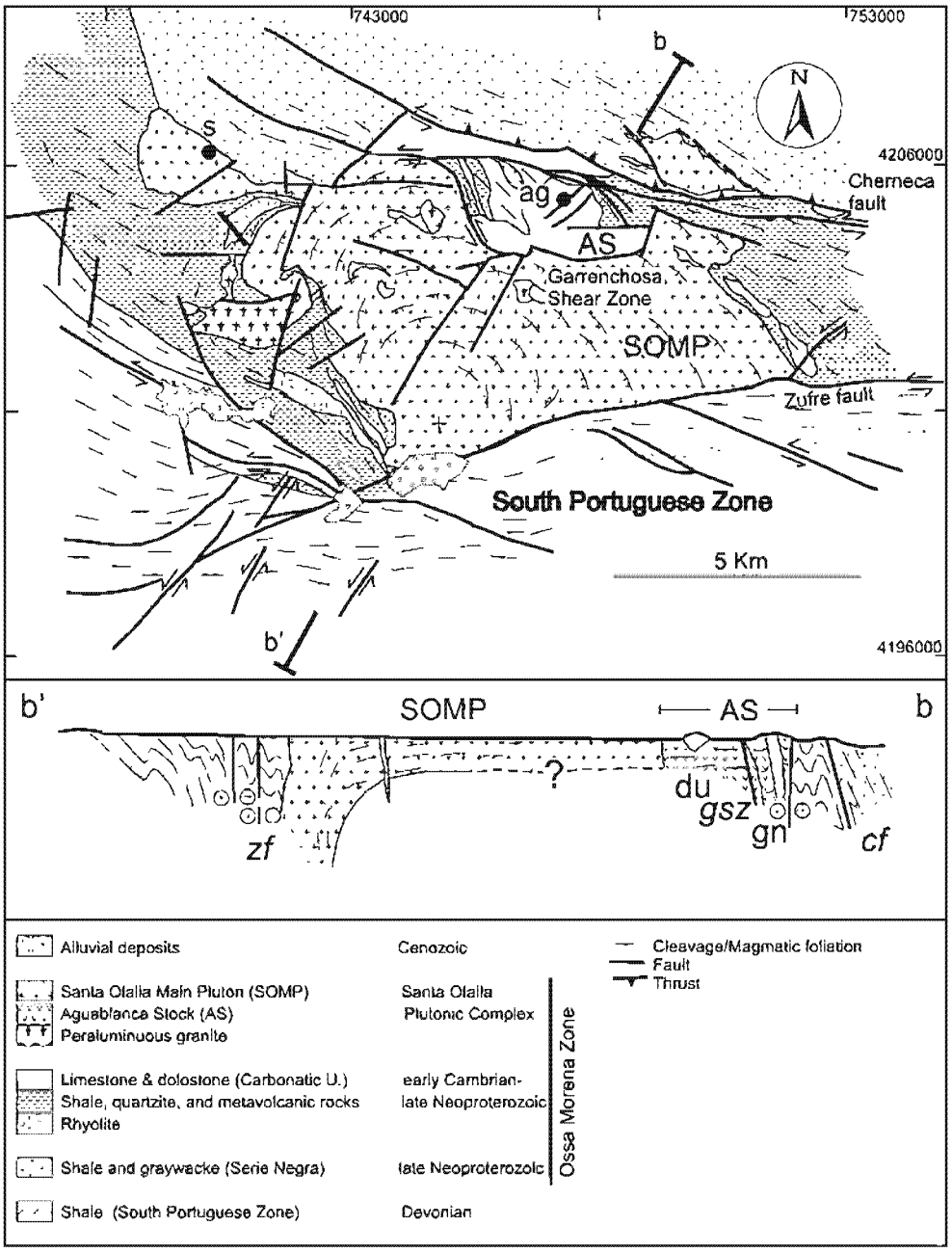

Fig. 2 Geologic map of the Santa Olalla Plutonic Complex. Modified from Casquet (1980) and ITGE (1990). Grid in UTM coordinates. An interpretative cross section (b–b') is exposed below showing the likely existence of two feeder zones for the intrusions. *zf* Zufre Fault, *cf* Chemeca Fault, *gsz* Garrenchosa Shear Zone, *SOMP* Santa Olalla Main Pluton, *AS* Aguablanca Stock, *gn* Gabbronorite Unit and breccia, *du* Diorite Unit, *ag* Aguablanca Mine, *s* Sultana Cu–(Au) Mine

Orthopyroxene is poikilitically included in the larger clinopyroxene crystals, suggesting that its crystallization began earlier than that of clinopyroxene. The orthopyroxene composition is rather monotonous ($en_{78–92}$) and shows low NiO contents (0.01 0.06 wt%) (see Electronic supplementary material). Clinopyroxene has a more variable composition (diopside and Mg augite) and has similar low NiO contents (<0.12 wt%). Plagioclase phenocrysts show normal zoning with cores of variable composition between an_{56} and an_{90} (bytownite labradorite) and rims of oligoclase andesine ($an_{24–35}$). Olivine is very scarce and only occurs as scattered anhedral unzoned grains mantled by plagioclase and pyroxene. Phlogopite (X_{phlog}, 0.49 0.70) and clinoamphibole (magnesiohornblende-actinolite) occur as interstitial 0.5- to 2-mm-sized anhedral crystals along with quartz (Fig. 4a). Accessory igneous minerals are ilmenite, rutile, pyrrhotite, and apatite. The pegmatitic gabbro consists of actinolite-hornblende, diopside, and oligoclase ($an_{16–24}$) and minor quartz, muscovite, titanite, allanite, and apatite.

The Aguablanca Stock has abundant xenoliths of the host rocks, ranging in size from centimeters to several meters, particularly garnet-pyroxene skarn and pelitic and calc-silicate hornfels. There are fairly abundant but small peraluminous microenclaves that contain oligoclase, biotite, spinel, cordierite, corundum, sillimanite, and K-feldspar.

Table 1 Major lithologic units of the Santa Olalla plutonic complex, SW Spain

Intrusion & intrusive unit	Occurrence	Composition	Mineralogy	Texture	Hydrothermal alteration	Age (Ma)
Santa Olalla Main Pluton						
	Large (km-sized) ellipsoidal intrusion with reverse zonation. Subtle subhorizontal magmatic foliation	Monzogranite–granodiorite in the core grading to tonalite and diorite and Q-diorite in the rim	plag, bt, amph, Q, kf, (ap, zr, ilm, rut). Only accessory sulfides (po)	Massive, granular, medium- to coarse-grained	Negligible	332±3[a] 341±3[2] 347.0±[3].4[3]
Aguablanca Stock						
Diorite Unit	Dominant in the stock. Subhorizontal magmatic foliation	Bt-, amph-bearing diorite, and Q-diorite	plag, cpx, amph, bt (Q, ap, zr). Scarce sulfides disseminated and in veinlets	Massive, granular, coarse- to medium-grained. Local subophitic textures	Minor. Sericitization plag. Replacement px by amph. Most sulfides of hydrothermal origin	338.6±0.8[b]
Gabbro–norite Unit	Located in the N area of the Stock. Gradual contacts. Subhorizontal to subvertical magmatic foliation	Norite, gabbronorite, and pyroxenitic gabbro	opx, cpx, plag (bt, amph, ol, Q, ilm, rut, ap, sp). Sulfides disseminated, patches and veinlets forming locally significant mineralization	Massive, medium-grained. Local cumulates	Intermediate. Local texturally destructive. Sericitization plag. Replacement px by amph. Endoskarn. Some hydrothermal mineralization	344.0±1.1[c] 338.2±1.7[d] 338.2±3.0[d]
Breccia pipe	Hosted by the Gabbro–norite Unit forming a subvertical pipe with gradual contacts	Heterometric fragments of pyroxenitic and accessory peridotitic cumulates. Fragments of host rocks. The fragments are usually unmineralized	opx, cpx, bt, amph (plag, ol, sp). Sulfides massive and disseminated. Abundant veinlets	Dominant cumulates (ultramafic). Fragments randomly oriented but local flow textures	Extensive. Local texturally destructive. Sericitization plag. Replacement px by amph. Endoskarn	335±2[d]
Barren breccia	Usually external zone of the breccia pipe	Fragments of the breccia pipe cemented by rocks of the Gabbro–norite Unit			Extensive. Local texturally destructive. Sericitization plag. Replacement px by amph. Endoskarn	
Ore breccia	Internal zone of the breccia pipe	Fragments of the breccia pipe cemented by sulfides with more accessory gabbro–norite			Irregular recrystallization of magmatic sulfides	
Massive sulfides	Included in the ore breccia as large, randomly distributed masses	Massive–semimassive sulfides with disseminated pyroxene crystals			The pyroxenes are only slightly altered. Widespread retrogradation of magmatic sulfides	
Cortegana Complex						
	Large sills in the Aracena Massif	Highly heterogeneous tonalite–diorite with norite–gabbro and ol–websterite, lherzolite, dunite, orthopyroxenite. Minor harzburgite, troctolite, and wehrlite	ol, opx, cpx, bt, amph (plag, sp). Abundant disseminated sulfides	Dominant cumulates in the mafic–ultramafic rocks. Coarse-grained	Widespread evidences of major fluid circulation	321.5±33[d] 336.2±1.7[d]

amph Clinoamphibole, *ap* apatite, *bt* biotite, *cpx* clinopyroxene, *ilm* ilmenite, *kf* K-feldspar, *ol* olivine, *opx* orthopyroxene, *plag* plagioclase, *po* pyrrhotite, *Q* quartz, *rut* rutile, *sp* spinel, *zr* zircon

[a] Montero et al. (2000) (U–Pb)

[b] Romeo et al. (2004) (U–Pb)

[c] Spiering et al. (2005) (U–Pb)

[d] This study

Table 2 Representative chemical analyses of samples from the Aguablanca Stock and the Cortegana Complex

	AG-207-2	AG-156	AG-159	AG-160	AB-37	AG-97	SO-32	AG-85	AG-213	SO-57	SO-56d	TE-4	TE-12	TE-9
	Breccia ore				Gabbronorite Unit					Diorite Unit		Cortegana Complex		
	Pyroxenite		Norite		Gabbronorite		Gabbro		Contact Gabbro	Diorite		Norite	Gabbro	Websterite
SiO_2	50.88	52.44	53.67	52.64	53.25	53.46	51.80	53.60	52.09	55.00	57.10	51.60	53.36	46.20
Al_2O_3	14.00	7.71	7.24	9.17	10.22	8.10	13.00	9.95	13.70	15.00	15.60	14.11	14.32	6.48
FeO_t	5.94	10.84	9.62	9.34	8.04	8.96	7.94	8.14	5.94	7.45	6.31	9.51	6.93	14.02
MnO	0.15	0.20	0.19	0.18	0.19	0.22	0.16	0.18	0.12	0.16	0.12	0.17	0.14	0.25
MgO	11.12	17.64	18.69	16.98	17.50	19.13	14.00	15.92	13.59	7.69	5.59	11.93	9.70	24.78
CaO	12.24	6.74	6.12	7.01	7.04	6.08	8.71	6.65	8.75	6.76	6.07	7.68	10.11	3.67
Na_2O	1.59	1.07	1.09	1.46	1.15	0.98	1.64	1.44	1.75	3.22	3.49	1.27	2.55	0.61
K_2O	0.62	0.48	0.59	0.65	0.54	0.56	0.52	0.74	0.89	1.49	2.40	0.54	0.55	0.39
TiO_2	0.37	0.36	0.32	0.50	0.24	0.36	0.58	0.33	0.32	0.82	0.72	0.21	0.23	0.32
P_2O_5	<0.05	0.02	0.02	0.07	0.02	0.03	0.04	0.09	0.02	0.13	0.12	<0.05	0.03	<0.05
S	(*)	0.27	0.05	0.09	0.06	0.09	(*)	(*)	(*)	(*)	(*)	(*)	0.69	(*)
LOI	2.49	1.32	1.38	0.96	0.93	1.13	0.93	2.41	2.18	0.62	0.93	1.93	1.33	2.72
Total	99.87	99.23	99.23	99.27	99.38	99.43	99.55	99.69	99.63	98.57	98.66	100.20	100.47	101.20
Rb	32	17	22	21	22	22	25	31	36	59	81	16.7	13	10
Sr	347	173	154	213	219	170	319	260	278	318	339	289	214	124
Ba	256	121	144	160	98	129	211	174	206	494	594	98	110	86
V	40	191	131	164	108	128	204	125	97	186	188	119	194	65
Cr	609	1410	1473	1252	1176	1394	880	1110	1084	510	250	4.05	211	118
Co	79	75	60	61	63	68	58	64	64	9	31	108	38	147
Ni	1888	539	454	431	419	525	292	348	444	202	78	366	173	1190
Cu	1158	177	60	67	66	122	66	61	407	68	85	175	85	154
Zn	33	56	70	57	54	66	93	73	38	108	75	76	44	78
Y	27	11	10	15	7	10	12	12	10	10	40	49	13	8
Nb	<0.6	2.2	2.2	2.8	1.4	2.1	10.0	2.4	1.2	14.0	30.0	2.5	<10	1.1
Zr	35	23	17	22	17	19	39	57	38	128	169	53	58	27
Pb	21	3	8	5	10	7	3	5	10	9	32	3	<10	4
U	2.2	0.51	0.68	0.50	0.44	0.49	0.50	0.87	1.3	1.40	1.50	<0.1		<0.1
Th	<1	1.40	2.09	1.53	1.31	1.58	1.10	3.12		4.20	10.00	<1		<0.8
La	9.8	5.9	6.2	7.7	4.9	5.8	7.6	8.4	7.2	25.1	25.9	13.6		2.6
Ce	18.9	13.6	13.5	18.0	10.2	13.0	17.0	17.5	14.0	51.0	52.0	24.4		5.8
Pr	2.6	1.7	1.7	2.3	1.2	1.6		2.1	1.6			3.3		0.7
Nd	12.7	7.3	7.0	10.9	4.6	6.4	9.0	8.4	6.7	21.0	25.0	12.5		3.0
Sm	3.5	1.9	1.7	2.8	1.1	1.5	2.1	2.0	1.5	4.3	5.1	3.7		1.0
Eu	1.1	0.5	0.4	0.7	0.4	0.4	0.7	0.6	0.4	1.4	1.1	0.4		0.3
Gd	3.9	1.9	1.7	2.6	1.0	1.5		2.0	1.4			4.8		0.9
Tb	0.6	0.3	0.3	0.4	0.2	0.2	0.5	0.3	0.2	0.7	0.7	0.9		0.2
Dy	3.8	1.9	1.6	2.6	1.1	1.5		2.1	1.2			6.0		1.0
Ho	0.8	0.4	0.4	0.6	0.3	0.3		0.4	0.1			1.3		0.2
Er	2.1	1.1	1.0	1.5	0.8	0.9		1.3	0.7			4.2		0.6
Tm	0.3	0.2	0.2	0.2	0.1	0.2		0.2	0.1			0.9		0.1
Yb	1.7	1.1	1.1	1.4	0.8	0.9	1.3	1.40	0.8	2.5	2.6	5.6		0.8
Lu	0.3	0.2	0.2	0.2	0.1	0.1	0.2	0.2	0.1	0.4	0.4	0.9		0.1

Analysis IGME
LOI Loss on ignition
All Fe as FeO_t
(*) Included in LOI
Major elements in weight percent (wt%); trace elements in parts per million (ppm)

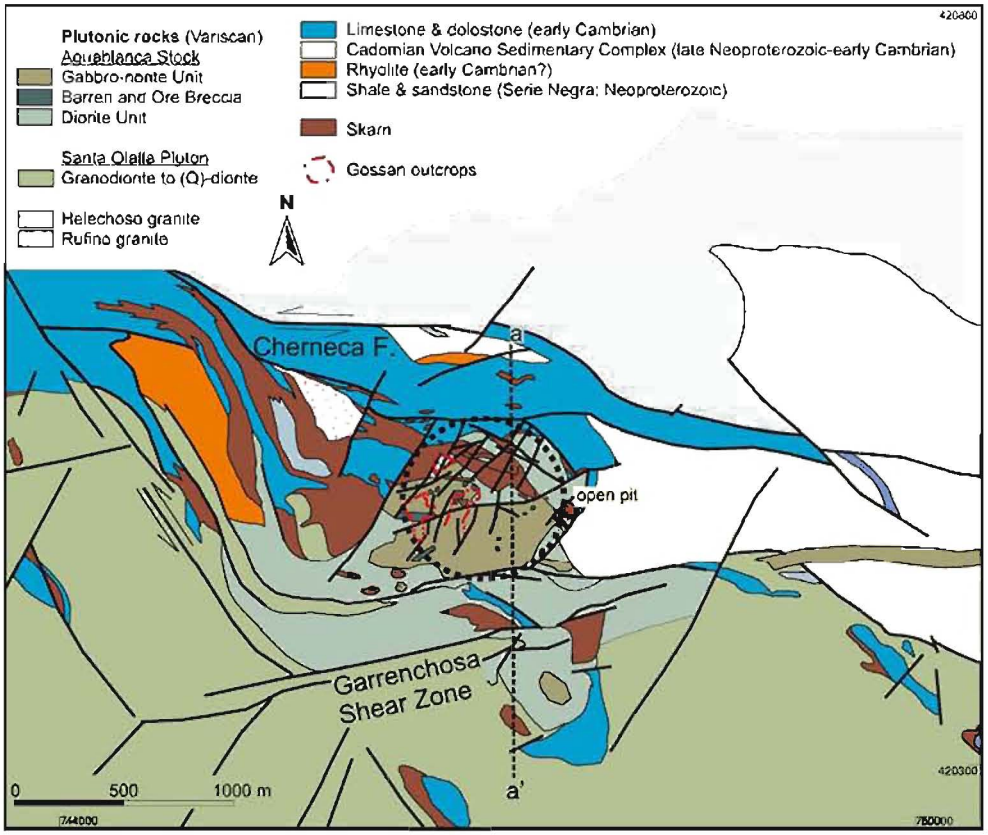

Fig. 3 Detailed premining geologic map of the Aguablanca orebody. Modified from Tornos et al. (2001) and Spiering et al. (2005). Grid in UTM coordinates

Spinel forms clusters of green euhedral crystals included in plagioclase. Electron microprobe (EPMA) analyses show that it is a ferriferous aluminum spinel (FeO_t=19.9 22.7 wt%) characterized by low Cr (<0.05 wt% Cr_2O_3), Ni (<0.31 wt% NiO), and Ti (<0.1 wt% TiO_2) contents. This composition, the absence of plagioclase rims, and the relationship with peraluminous assemblages strongly suggest that the spinel phase corresponds to insoluble relicts of assimilated xenoliths. The spinel composition differs from those of igneous spinel in magmatic Ni Cu deposits (Barnes and Tang 1999) but is similar to that recognized in the Voisey's Bay Ni (Cu Co) deposit where assimilation of crustal pelitic material was important (Kerr and Ryan 2000; Li and Naldrett 2000).

The Gabbronorite Unit, as well as to a lesser extent the Diorite Unit, also contains irregularly distributed centimeter-sized ellipsoidal enclaves of sulfide-bearing pyroxenite that is equivalent to those of the breccia pipe which is described below.

Application of the geothermometer based on the enstatite-diopside solvus (Bertrand and Mercier 1985) in the Gabbronorite Unit yields consistent values between 940 and 1,120°C. For these temperatures, the pyroxene geobarometry (Nimis 1999) indicates pressures of 4.3 to 5.7 kbar. P T values recorded here probably correspond to those of the differentiating magma chamber that underlies the Santa Olalla Plutonic Complex (see below).

The Aguablanca orebody

The Ni (Cu) Aguablanca deposit consists of two E W steeply northward dipping ellipsoidal orebodies hosted by the Gabbronorite Unit (Figs. 3, 5 and 6). The southern orebody is the largest one, with a surface of approximately 360×300 m^2, and has been traced down to a depth of 550 m. The northern orebody is significantly smaller, 300×100 m^2, and extends downward for at least 160 m. The extension below these ore zones is not well understood due to the limited amount of deep drill holes but it seems that they grade into a gently dipping high-grade mineralized zone (1 wt% Ni) averaging 30 70 m in thickness (Spiering et al. 2005).

Four types of ore have been distinguished: ore breccia, massive sulfides, disseminated ore, and patchy ore. Ore breccia and massive sulfides are only found in the southern orebody, whereas the northern orebody includes patchy and disseminated ores. The relationships among the different types of ore are obscure because most of the contacts are tectonic (Figs. 5 and 6). The pattern that emerges in the southern orebody is one of a telescoped arrangement, with disseminated and patchy ore in an outer disposition and pipe-like breccia bodies and massive sulfides as inner lenses.

Most of the ore (50 60%) occurs as disseminations in rocks belonging to the Gabbronorite Unit. Sulfides (5 20% of the rock volume; 0.1 10 mm in size) are interstitial to plagioclase and pyroxene and intergrown with phlogopite and

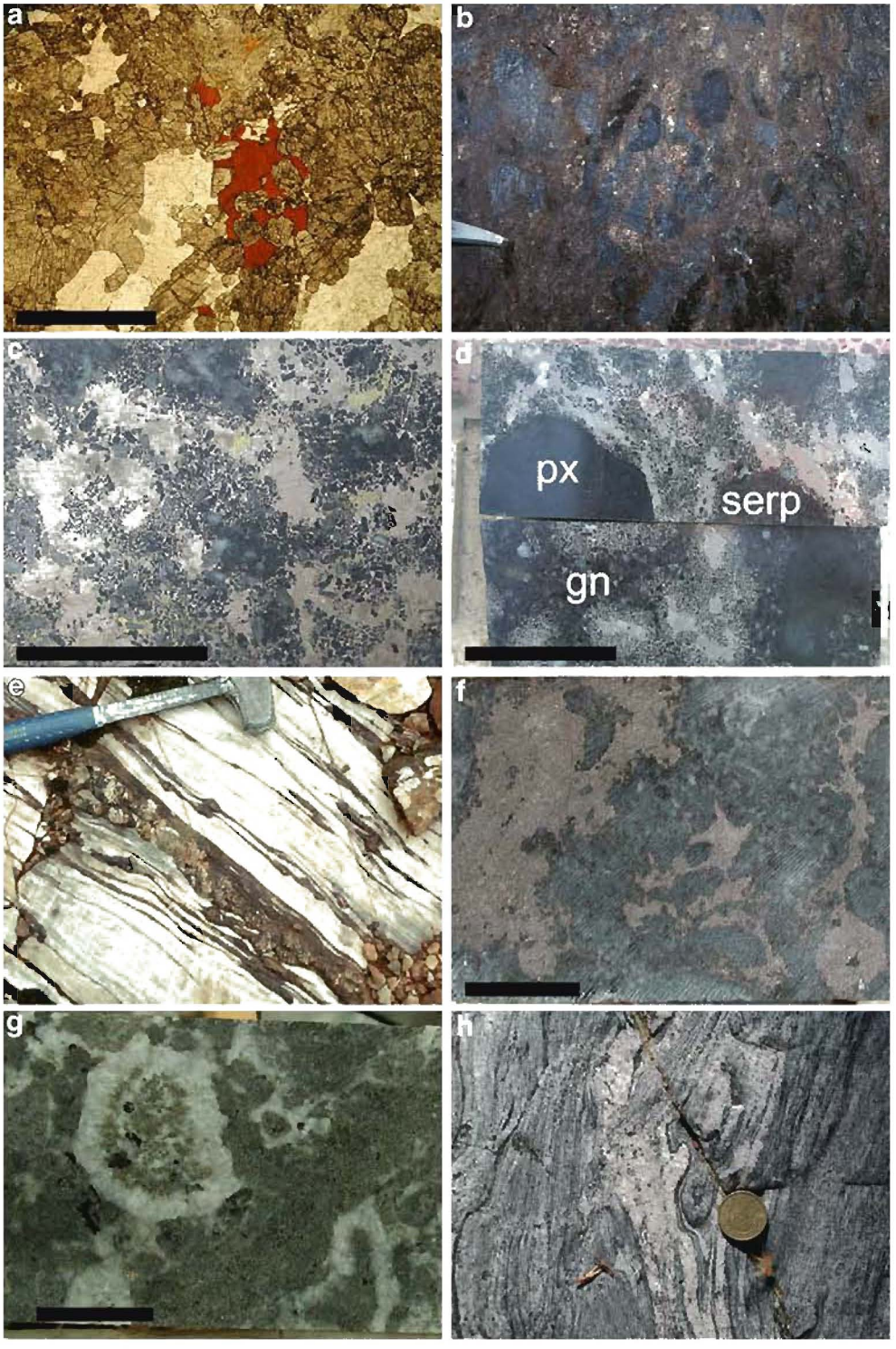

Fig. 4 Photographs of the host rocks and mineralization at Aguablanca and Cortegana. **a** Norite with cumulus texture and abundant intercumulus phlogopite. Sample AG-135. *Scale bar*: 1 mm. **b** Ore breccia. Fragments of fine-grained pyroxenite (*dark gray*) supported by massive sulfides and some coarse-grained gabbro to norite. **c** Semimassive sulfides made up of pyrrhotite, chalcopyrite, and pentlandite. They have abundant, unevenly dispersed crystals of ortho- and clinopyroxene and irregular intergrowths of coarse-grained gabbro to norite. This rock and the sulfides are interpreted as derived from immiscible melts. *Scale bar*: 3 cm. **d** Ore breccia. Fragments of fine-grained pyroxenite (*px*) and serpentinite (*serp*) supported by irregularly mixed sulfides and gabbronorite (*gn*). The pyroxene crystals tend to concentrate near the fragments. *Scale bar*: 1 cm. **e** Sheared calcitic marble with highly strained garnet-rich skarn within the Cherneca Fault. **f** Cortegana Igneous Complex. Intercumulus pyrrhotite in pyroxenite. *Scale bar*: 2 cm. **g** Orbicular gabbro forming the lowermost part of the Cortegana Igneous Complex. *Scale bar*: 3 cm. **h** Anatexite in the footwall of the Cortegana Igneous Complex

amphibole. The grades are up to 1% Ni+Cu, and the Ni/(Ni+Cu) ratio is close to 0.3 0.5. Patchy ore is similar to the disseminated ore, although the sulfides occur in dispersed blebs about a centimeter in diameter. It comprises 20 35% of the total ore volume and has irregular grades, usually below 0.7% Cu+Ni. Moreover, the Gabbronorite Unit also includes scattered meter-sized lenses of massive sulfides (Fig. 7).

Ore breccia and massive sulfides comprise 15 20% of the total orebody volume. Copper grades are equivalent to those of disseminated and patchy ore but there is an up to fivefold enrichment in Ni, which is usually higher than 1% (Ortega et al. 2004). Because of their genetic and economic importance, the ore breccia and the massive sulfides are described in detail below.

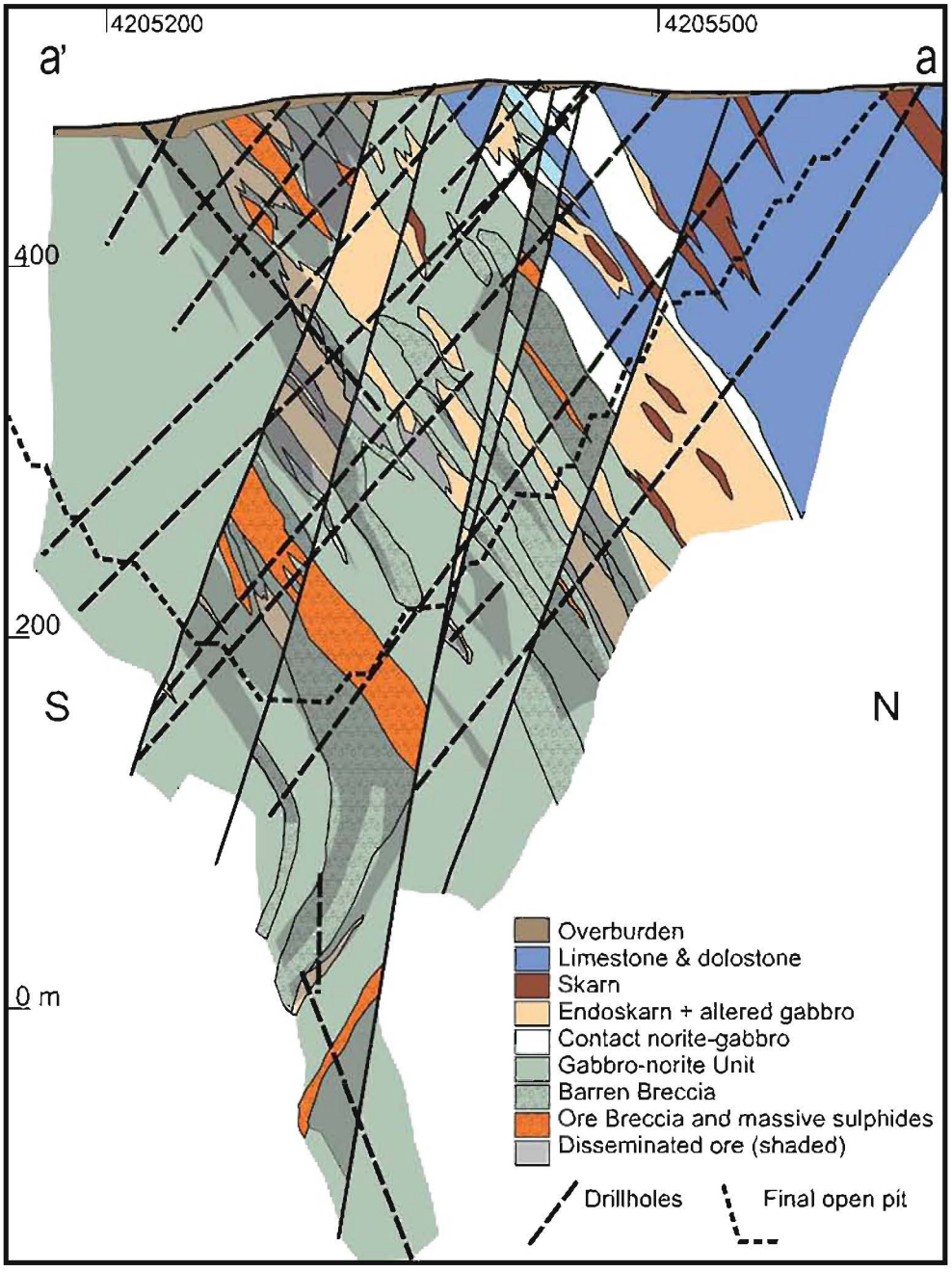

Fig. 5 Interpretative N–S cross section (a–a' in Fig. 3) of the Aguablanca orebody showing the distribution of the mineralization. Modified from Spiering et al. (2005)

As a whole, the orebody has a Ni/(Cu+Ni) ratio of 0.43. This ratio is equivalent to that of other gabbro-hosted deposits like Voisey's Bay (0.45 0.75; Naldrett 1999). Cu and Ni show a positive correlation (r=0.78), a feature probably inherited from a liquid monosulfide solution and unlikely to result from Cu input during later hydrothermal alteration. Cobalt has a positive but weak correlation with Ni and Cu (r=0.04 0.07).

The Ni and Cu contents and the Ni/(Ni+Cu) ratio are quite variable throughout the orebody, and no vertical or horizontal chemical zonation is evident. Also, there is no increase in grade or change in the style of mineralization toward the contact with the host rocks; in fact, the rocks adjacent to the contact, including the skarn, are usually barren, and only a few bodies of massive magnetite or pyrrhotite are found. No metasomatic ore, similar to that described at Jinchuan by Chai and Naldrett (1992), has been found in the host rocks or within the xenoliths in the Aguablanca Stock.

Breccias and massive sulfides

The breccia bodies are discontinuous and have a pipe-like geometry with a roughly elliptical, up to 30×10 m^2, section. The lenses are roughly parallel to the stock contact

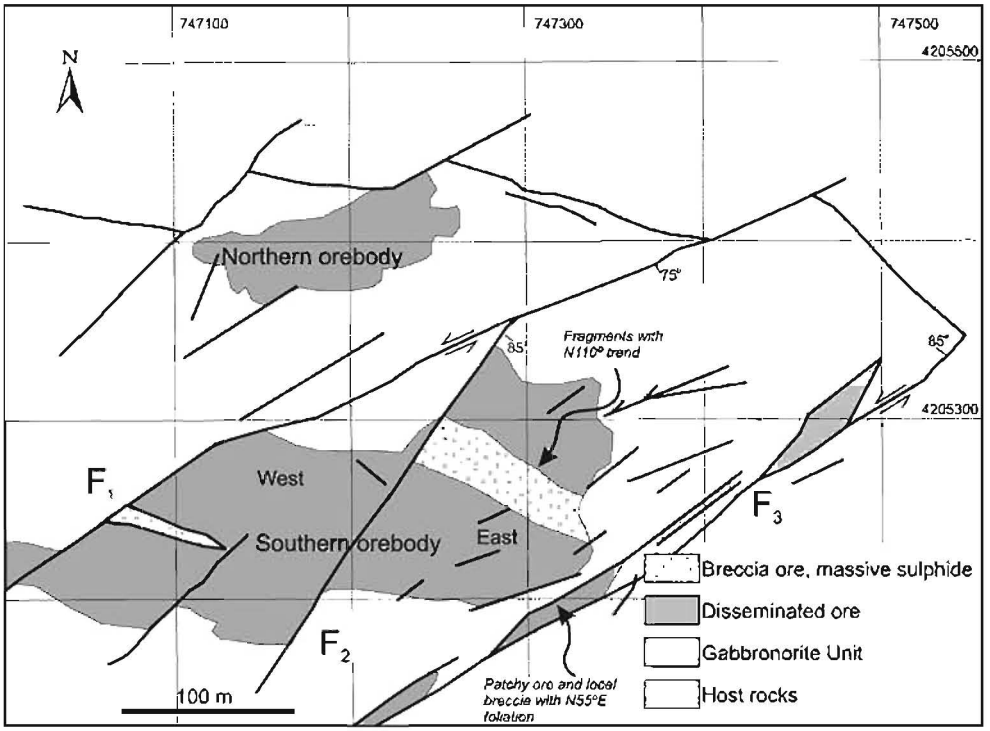

Fig. 6 Plan of the 485-m level of the Aguablanca mine showing the relationships between the different orebodies and faults

(N100 120°E) and dip 45 80°NE (Fig. 5). The breccia consists of poorly sorted heterolithic subangular to subrounded fragments supported dominantly by sulfides (ore breccia) or by gabbronorite (barren breccia) (Figs. 4b d and 8). The barren breccia dominates in the northern orebody, while ore breccia is restricted to the southern orebody.

The proportion of fragments is very variable. There are rocks with evenly dispersed fragments to fragment-supported breccias with fragments forming up to 60 70% of the total rock volume. Their size is usually between 1 and 20 cm, but sporadic clasts up to some meters across can be found. Reaction rims are uncommon, and the fragments show sharp contacts with the supporting matrix.

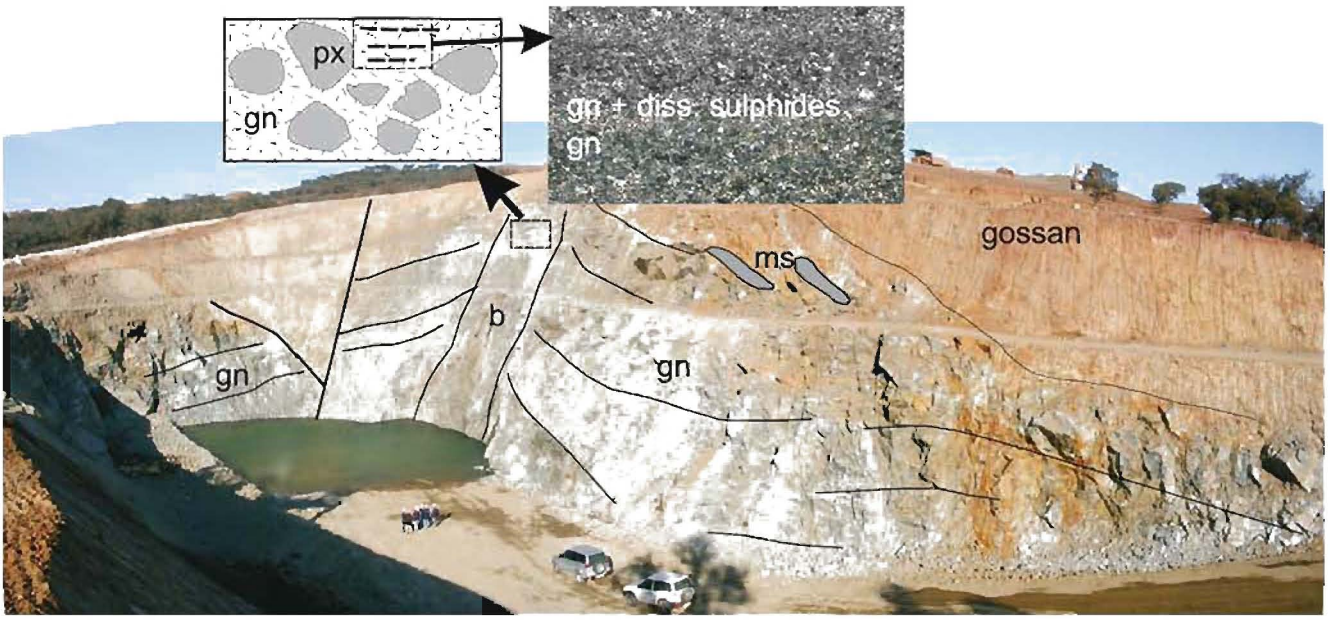

Fig. 7 Crosscutting relationships between the Gabbronorite Unit and the breccia in the northern orebody. The breccia (*b*) dissected the Gabbronorite Unit (*gn*), verticalizing the originally subhorizontal magmatic layering. The Gabbronorite Unit hosts some lenses of massive sulfides (*ms*). The uppermost part of the breccia bodies show centimeter-sized subhorizontal cumulate textures with pyroxenite fragments (*px*) supported by gabbronorite with disseminated ore

Fragments include:

(a) fine-grained (0.05 0.5 mm) massive pyroxenitic orthocumulate with no signs of internal deformation. The pyroxenite consists of subeuhedral to euhedral orthopyroxene (en_{76-79}; NiO<0.1 wt%) and clinopyroxene (diopside-augite) in variable proportions with only minor plagioclase and abundant intercumulus phlogopite and clinoamphibole (fluor ferroedenite to magnesiohornblende). The pyroxenite fragments are poor in sulfides, and only little low-Ti magnetite and pyrrhotite occur.

(b) Host rock xenoliths, including calcic and magnesian skarns, pelitic and calcsilicate hornfels, and minor marble.

(c) Fine-grained gabbro, similar to the Contact Gabbro of the Aguablanca Stock.

(d) Rare peridotite fragments that consist of forsteritic olivine (fo_{86-93}; NiO=0.01 0.18 wt%), sometimes poikilitically included in orthopyroxene, and Mg-rich phlogopite (X_{phlog}=0.61 0.83). Olivine crystals surrounded by a kelyphitic rim of clinopyroxene, plagioclase, and spinel were described by Lunar et al. (1997).

(e) Serpentinite consisting of reniform to nodular serpentine with interstitial chlorite and Ti- and V-poor magnetite, graphite, and pyrrhotite. The intercumulus texture of the magnetite and sulfides suggests that these enclaves are altered peridotitic cumulates and are not retrograded magnesian skarn.

(f) Rare plagioclase-rich fragments, composed of subhedral plagioclase (an_{95-100}); the origin of these rocks is unknown and could well be a true anorthosite or a plagioclase-rich endoskarn similar to that found in the immediate vicinity of the stock. Piña et al. (2004) have also mentioned fragments of olivine-bearing gabbro and troctolite that have not been found in this study. The first two types of fragments account for more than 95% of the total clasts in the breccia. The barren breccia includes abundant fragments of partially digested host rock, while the ultramafic fragments dominate in the ore breccia.

The supporting groundmass of the breccia consists of either massive sulfides or coarse-grained gabbronorite with disseminated sulfides. Both sulfides and silicates are irregularly intergrown as centimeter- to meter-sized irregular masses with curved irregular to cuspated contacts that are unlikely for fragments and strongly suggest the presence of immiscible sulfide and silicate magmas (Fig. 8).

Massive sulfides occur as meter-sized lenses within the breccia and consist of coarse-grained pyrrhotite pentlandite with irregular masses and veins of chalcopyrite and only evenly dispersed fragments. Dispersed in the massive sulfides, preferentially near the fragment margins, there are abundant millimeter-sized euhedral crystals of orthopyroxene (en_{74-87}; NiO<0.1 wt%) and diopside-augite in addition to some plagioclase and phlogopite. These pyroxene crystals are typically unoriented but have developed a glomeroporphyritic texture. However, they locally define a flow banding wrapping large fragments. These rocks are called leopardite in mine terminology.

The pipe-like morphology of the breccia bodies, the crosscutting relationships with the host Gabbronorite Unit, the polymictic nature of the fragments, and the presence of steeply dipping magmatic flow banding are all consistent with a highly dynamic mechanism of intrusion.

Figure 7 shows the crosscutting relationships between the different units in the NE area of the orebody. They show that the breccias are younger than the gabbronorite hosting the disseminated ore. The subhorizontal layering in the Gabbronorite Unit gradually displays steepness toward the barren breccia of the northern orebody, showing that the breccia disrupted an already layered but still ductile gabbronorite. Crosscutting relationships between the Diorite and Gabbronorite Units are unclear but the presence of enclaves of the latter in the diorite suggests that the Diorite Unit is younger than the Gabbronorite Unit.

Breccias similar to those of the Aguablanca deposit are fairly common in magmatic Ni (Cu) deposits. They have been interpreted as zones of incomplete assimilation of the host rocks, sometimes in erosional channels in the footwall of magmatic complexes (e.g., Sudbury; Lightfoot et al.

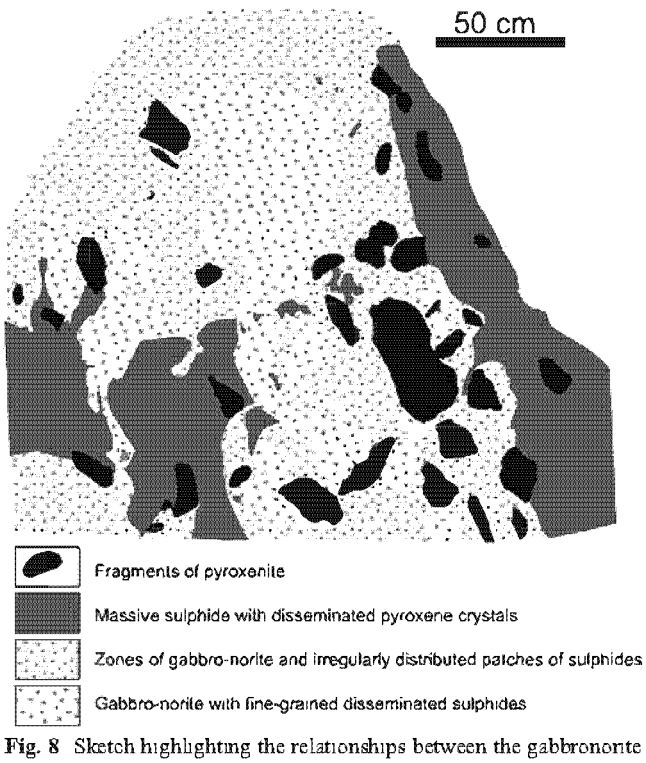

Fig. 8 Sketch highlighting the relationships between the gabbronorite and sulfide cement in the breccia

1997b), as collapse breccias in the top of intrusions (Noril'sk; Naldrett 1992) or as feeder zones to overlying plutons (e.g., Voisey's Bay; Ryan 2000). The spatial relationships with the host rocks and the relative timing make the breccia at the Aguablanca deposit somewhat similar to the Composite Gabbro or the Ovoid Conduit of Voisey's Bay, characterized by its subvertical morphology and the presence of gabbro with disseminated mineralization that is crosscut by the massive sulfides (Kerr and Ryan 2000). However, an uncommon feature of the breccia at the Aguablanca deposit is the relatively xenolith-poor character if compared with those described elsewhere.

The magmatic ore assemblage

The main sulfide mineralization intergrown with primary magmatic silicates shows two superimposed mineral assemblages. An earlier assemblage of massive pyrrhotite with inclusions of pentlandite and chalcopyrite (stage I) was variably replaced by later coarse-grained chalcopyrite, pyrrhotite, and pentlandite (stage II). Stage I pyrrhotite occurs as 0.2–3 mm (exceptionally 5 mm) anhedral grains; XRD spectra of this pyrrhotite display an irregular crest instead of the typical 102 peak. This pattern is consistent with partial retrogradation of hexagonal pyrrhotite to a monoclinic phase during subsolidus reequilibration (Arnold 1969). Pyrrhotite exsolved pentlandite in droplets or, more frequently, in 50- to 100-μm-sized flames (Fe/Ni=0.96–1.08) along grain boundaries or within microfractures. As for many other equivalent systems, this early assemblage is interpreted as having formed through the exsolution of a monosulfide solid solution $(Fe, Ni, Cu)_{1-x} S_x$ during the early crystallization of a parental sulfide melt (e.g., Chai and Naldrett 1992; Ebel and Naldrett 1996).

However, most of the economic mineralization seems to be younger. Here, chalcopyrite, pyrrhotite, and pentlandite occur as coarse-grained aggregates (1–5 mm) that replaced early pyrrhotite or formed independent intercumulus or massive facies. Chalcopyrite occurs as subrounded grains that locally include small grains of cubanite, euhedral cobaltite, magnetite, and graphite. Pyrrhotite, lacking exsolved pentlandite, occurs as coarse grains interlocked with pentlandite and, to a lesser extent, with chalcopyrite. Pentlandite (Fe/Ni=0.8–1.2) occurs as inclusion-free, highly fractured independent grains between coetaneous pyrrhotite and chalcopyrite, or as veins within the latter. Evolution from early pyrrhotite-rich ores to later chalcopyrite-rich ones is typical of magmatic Cu–Ni deposits and is an expected consequence of fractional crystallization of sulfide melts (e.g., Naldrett 1989). The scarcity of Co-bearing minerals suggests that most of the Co is in the pentlandite lattice.

The relative timing of the magmatic mineralization can be established from petrographic relationships. Orthopyroxene and olivine are usually devoid of sulfide inclusions but are usually rimmed by sulfides; symplectitic intergrowths of pyrrhotite–orthopyroxene occur only locally. Moreover, the presence of abundant droplets of pyrrhotite in clinopyroxene suggests that sulfide immiscibility took place synchronously with the crystallization of orthopyroxene but predated the crystallization of clinopyroxene.

Abundant subhedral to anhedral magnetite occurs during intercumulus phase to pyroxene but earlier than the sulfides. Magnetite is Ti-rich (up to 1.2 wt%; see Electronic Supplementary Material) and locally carries exsolved ilmenite needles. Similar Ni-, Cr-, and Al-poor magnetite has been reported at Sudbury (Barnes and Tang 1999). Some ilmenite crystals are also observed but their relationship in the paragenetic sequence is not fully understood.

The sulfides exhibit a subtle deformation, and pyrrhotite and pentlandite show tectonic twinning and brecciation near major faults only.

Hydrothermal and supergene alteration

The Aguablanca Stock underwent an irregular but pervasive polyphase hydrothermal alteration. Most of the rocks show a subtle alteration with irregular replacement of primary mafic minerals by phlogopite (X_{phlog}, 0.68–0.74) and actinolite/magnesiohornblende (Fe/Fe+Mg, 0.07-0.52; see Electronic supplementary material) and of plagioclase by sericite, calcite, and chlorite.

However, alteration is particularly intense near the faults and lithologic contacts, predominantly affecting the plagioclase-bearing rocks, with the texturally destructive assemblage of clinoamphibole, biotite, clinozoisite (X_{ep}=0.02–0.03), quartz, and sulfides. Typical trace minerals are apatite, titanite, and zircon. The proportion of hydrothermal sulfides is quite variable, ranging from semimassive to disseminations or veinlets in altered gabbronorite. The sulfide assemblage is dominated by coarse-grained chalcopyrite and pyrite with only random inclusions of pyrrhotite and sphalerite. Bravoite and mackinawite are present as small grains, the latter replacing pentlandite. There is a characteristic late assemblage of magnetite–pyrite–graphite.

Ortega et al. (1999, 2004) have carried out an extensive study of the platinum group-bearing minerals and related phases. In Aguablanca, these minerals are found as grains of between 1 and 15 μm (exceptionally up to 45 μm) and consist of Pd- and Pt-bearing tellurides usually associated with Ag and Bi tellurides and native gold. The location of these minerals in fractures or on grain edges of pyrrhotite and pyrite strongly suggests that they are of hydrothermal origin and probably related to the retrograde alteration of

the magmatic sulfides, by which PGE contained as solid solution became liberated. This is consistent with the proton-microprobe studies of Czamanske et al. (1992) that show that early, high-temperature chalcopyrite and pentlandite can host significant amounts of Pd and Pt. A hydrothermal origin for the discrete PGE minerals in Cu–Ni deposits has been postulated by several authors (e.g., Mathez and Peach 1989).

A later hydrothermal event gave rise to irregular masses and veins of calcite, chlorite (clinochlore-pycnochlorite), phengite, talc, tremolite, quartz and sulfides, typically pyrite, chalcopyrite, mackinawite, and marcasite.

The hydrothermal alteration at Aguablanca is similar to that described elsewhere in magmatic Ni–(Cu) deposits (e.g., Ripley 1990), which has been interpreted as the major cause of Cu (Ripley et al. 1993) and PGE redistribution (e.g., Mathez 1989; Stumpfl 1993).

Supergene alteration is intense in the shallow part of the orebodies, with development of an earthy and soft goethite-, chlorite-, and clay-rich gossan up to 8–16 m in depth with grades up to 1% Ni; at near fractures, this supergene alteration reaches to depths of up to 60–80 m (Suarez et al. 2005). Incipient supergene alteration has altered pyrrhotite and pyrite to marcasite, magnetite to hematite, and chalcopyrite to chalcocite and covellite. Perhaps the most important aspect is the partial replacement of pentlandite by fine-grained violarite along grain edges and fractures. PGE minerals seem to be also concentrated in the supergene zone (Ortega et al. 2004).

The structural setting

Besides earlier Variscan folding and thrusting of the host sequence (Casquet 1980), the more important structures in the area are longitudinal strike-slip faults. The Santa Olalla Plutonic Complex is bounded by two first-order left-lateral strike-slip faults, i.e., the Cherneca Fault to the north and the Zufre Fault to the south (Figs. 1 and 2). The Cherneca Fault is associated with secondary antithetic faults that delimit blocks with a bookshelf geometry (Tornos et al. 2002b). A third structure, the Garrenchosa Shear Zone is found between the Santa Olalla Main Pluton and the Aguablanca Stock (Figs. 2 and 3), but mapping shows that it represents an anastomosing segment of the Cherneca Fault. The Garrenchosa Shear Zone includes a complex array of ENE–WSW sinestral shear zones that turn to the NNW–SSE west of the Aguablanca Stock. In detail, the Cherneca Fault and the Garrenchosa Shear Zone define an elongated structure 3 km long and up to 1.5 km wide, which hosts the Aguablanca Stock (Fig. 3). Mapping also shows that the regional cleavage and bedding of the host rocks generally wrap around the Aguablanca Stock, with dips between 50 and 70° outward.

The Santa Olalla Main Pluton displays gentle magmatic foliation that is subhorizontal or gently dipping inward. In the Aguablanca Stock, the foliation is less prominent but is also subhorizontal and trending N50 to N95°E. However, it changes to near vertical dips approaching the breccia bodies (Figs. 2 and 7), where both the flow banding in the massive sulfides and the orientation of the breccia fragments trace a subvertical magmatic foliation.

The Aguablanca Stock is densely fractured; however, the fractures do not extend away from the pluton into the host rocks. The more significant faults are subparallel to the Cherneca Fault, having strikes of N90–110°E and dips of 60° or more to the NE. The location of the orebodies seems to be controlled by left-lateral N35–55°E trending faults with steep dips (Fig. 6). Synthetic NW–SE trending faults, with a staircase geometry and 10 to 30-m spacing, branch out from the Cherneca Fault. Finally, there are WNW–ESE faults with dips close to 45°S; they seem to displace the mineralization at depth toward the south.

As a consequence of faulting, most contacts are tectonic, distorting the original morphology of the orebodies (Figs. 3, 5 and 6). Ongoing operation shows that three major strike-slip faults, the denominated F_1 to F_3, limit the mineralized area. F_1 and F_3 trend N50–60°E and dip steeply; F_1 marks the NW limit of the southern orebody, while F_3 bounds the SE limit. F_2 is a N40°E trending fault that splits the southern orebody in two different zones denominated west and east (Fig. 6). The F_3 structure hosts several ore pockets in extensional jogs indicating that it was active during the ore-forming process and controlled the emplacement of the orebodies.

Geochronology of the orebody

The age of the Aguablanca Stock and the hosted orebody has been one of the more controversial points for the regional geology, with implications to both the genetic interpretation of the deposit and mineral exploration models.

Two phlogopite concentrates, one from the gabbronorite cement from the ore breccia (AG-38) and another from a gabbro in the Gabbronorite Unit (AG-68), were selected for $^{40}Ar/^{39}Ar$ dating. Both rock samples contain abundant phlogopite that forms 1 to 3-mm-sized aggregates interstitial to plagioclase and pyroxene. Because the closure temperature for the diffusion of Ar is ca. 400°C, i.e., lower than the crystallization temperature of silicate magmas and the ore, $^{40}Ar/^{39}Ar$ dating of phlogopite provides minimum ages.

Phlogopite concentrates were irradiated for 50 h in packages KD32 and KD37 at the TRIGA reactor at the U.S. Geological Survey in Denver. Hornblende from the McClure Mountain Syenite (MMhb-1) with an age of 519.4±2.5 Ma (Alexander et al. 1978; Dalrymple et al. 1981) was used as a monitor mineral. The mineral concentrates were analyzed at

the USGS Argon Thermochronology Laboratory in Denver on a VG Isotopes Model 1200 B Mass Spectrometer fitted with an electron multiplier using the $^{40}Ar/^{39}Ar$ step-heating method of dating. For additional information on both analytical procedures and data reduction, see Kunk et al. (2001). We used the decay constants recommended by Steiger and Jäeger (1977). Plateau ages are identified when three or more contiguous steps in the age spectrum agree in age, within the limits of analytical precision, and contain more than 50% of the $^{39}Ar_K$ released from the sample. Average ages were calculated in the same manner as plateau ages except where contiguous steps do not agree. The $^{40}Ar/^{39}Ar$ step-heating values are listed in Table 3 and presented in Figs. 9 and 10.

The age spectrum for phlogopite AG-38 is fairly concordant but does not define a plateau. However, an isochron age of 335.0±2 Ma ($^{40}Ar/^{36}Ar_{initial}$=220±48; MSWD=0.63; 100% of total $^{39}Ar_K$ gas) was obtained. The age spectrum for phlogopite AG-68 is also fairly concordant but also does not define a plateau. However, a statistically well-constrained isochron age of 338.2±3.0 Ma was retrieved ($^{40}Ar/^{36}Ar_{initial}$=461±97; MSWD=0.47; 100% of total $^{39}Ar_K$ gas). Both phlogopite ages are coincident within the error limits between 335 and 337 Ma; thus, the age interval of coincidence probably corresponds to the age of cooling of the pluton and orebody below ca. 400°C.

These phlogopite Ar–Ar ages are consistent with the U–Pb zircon crystallization ages for the igneous rocks (Romeo et al. 2004; Spiering et al. 2005). Whole-rock K–Ar dating of the Gabbronorite Unit by Casquet et al. (1999) yielded two ages (325 and 307 Ma) that are significantly younger than the phlogopite Ar–Ar ages, suggesting that significant hydrothermal overprint occurred after the crystallization of the plutons.

Mafic–ultramafic intrusions of the Cortegana Igneous Complex

Bodies of mafic and ultramafic plutonic rocks, formerly mapped as "diorite", are widespread in the Aracena Massif. As quoted above, these intrusions probably correspond to exhumed portions of a deep magmatic complex located below the Ossa Morena Zone.

In the Cortegana area (Fig. 11), plutonic rocks, grouped in the Cortegana Igneous Complex, form lenses concordant with the subhorizontal foliation in the host migmatite (Fig. 4h). The lenses can be up to 600 m thick and are mainly composed of gabbro and norite. They host several, up to 100–150 m thick, units of ultramafic rocks, including olivine websterite, lherzolite, dunite, and orthopyroxenite; harzburgite, troctolite, and wehrlite are also found. Anorthosite locally occurs in the footwall of the ultramafic bodies. A contact zone, 15–300 m thick, consists of tonalite to diorite with abundant diffuse remnants of incompletely digested host rock. This outer hybrid contact facies grades into orbicular (quartz)-diorite and tonalite (Fig. 4g) and the innermost gabbro–norite. All the igneous rocks are coarse-grained, show a subhorizontal magmatic layering and cumulus textures, and have abundant intercumulus phlogopite and amphibole; xenoliths of skarn and of calc-silicate and pelitic hornfelses are common. Moreover, graphite is locally abundant and probably derived from the digestion of the graphite-bearing black quartzite interbedded in the Neoproterozoic metasedimentary sequence (Rodas et al. 2000). Hydrothermal alteration is pervasive and has produced an irregular retrograde mineral assemblage. All rocks are crosscut by aplitic to pegmatitic dykes of trondhjemitic composition, which probably represent partial melts derived from the host migmatite.

Recent exploration work by Rio Narcea SA (Spiering et al. 2005) has recognized several mineralized zones within the ultramafic cumulates. Mineralization consists of pyrrhotite and chalcopyrite with minor amounts of pentlandite. Bulk grades are low, near 0.16% Ni and 0.08% Cu, but there are narrow intervals with higher grades reaching up to 1.4% Ni and 0.2% Cu. The PGE contents are also very low at about 2–6 ppb combined PGE.

Phlogopite $^{40}Ar/^{39}Ar$ chronology

Two concentrates of phlogopite from quartz-diorite (TEJ-3) and websterite (ZOM-23) from the Cortegana Igneous Complex were dated by the $^{40}Ar/^{39}Ar$ method following the procedure described above (Table 3).

Sample TEJ-3, which is heterogeneous and shows evidence of interaction with the host migmatite, shows a disturbed age spectrum (Fig. 9). However, an isochron age of 321.5±32.6 Ma ($^{40}Ar/^{36}Ar_{initial}$=4,039±4,214; MSWD=0.06; 70.6% of total $^{39}Ar_K$ gas) was obtained. Sample ZOM-23 yielded a plateau age of 336.2±1.7 Ma (steps B through D; 58% of $^{39}Ar_K$). This age is supported by the less precise isochron age of 328.1±6.3 Ma. Both phlogopite ages record minimum ages for the crystallization of the igneous rocks and their sulfide mineralization in the Cortegana Igneous Complex and are within error of those found for the Aguablanca Stock. Because peak–metamorphic conditions in the Aracena Massif were attained between 342 and 328 Ma (hornblende $^{40}Ar/^{39}Ar$ ages; Dallmeyer et al. 1993; Castro et al. 1999), we infer that mafic/ultramafic magmatism in the Aracena Massif took place synchronously with the high-T low-P postorogenic metamorphism and was broadly coeval with the emplacement of the Santa Olalla Plutonic Complex at epizonal levels.

The synmetamorphic emplacement of the Cortegana Igneous Complex is evidenced by concordance of the

Table 3 $^{40}Ar/^{39}Ar$ step-heating data for phlogopite separates from Aguablanca and Cortegana, SW Spain

Step	T (°C)	^{39}Ar of total (%)	Radiogenic yield (%)	$^{39}Ar_k$ (mol × 10^{-12})	$\frac{^{40}Ar^*}{^{39}Ar_k}$	Apparent K/Ca	Apparent K/Cl	Apparent age (Ma)	Error (Ma)
(a) AG-38. Phlogopite. J=0.012248±0.50%. Wt.=2.5 mg. #36KD32									
A	1,000	5.6	95.7	0.01592	16.432	31.1	17	330.8	±2.0
B	1,050	7.1	98.8	0.02033	16.552	33.4	18	333.0	±1.7
C	1,100	6.4	99.0	0.01844	16.580	21.6	17	333.5	±1.9
D	1,150	9.2	99.2	0.02647	16.768	15.3	17	337.0	±1.1
E	1,200	14.9	99.5	0.04278	16.797	24.5	17	337.5	±0.8
F	1,250	29.4	99.7	0.08420	16.660	89.0	19	335.0	±0.5
G	1,300	27.4	99.8	0.07867	16.595	37.6	20	333.8	±0.4
Total gas		100.0	99.3	0.28681	16.647	47.0	18	334.8	
(b) AG-68. Phlogopite. J=0.012328±0.50%. Wt.=2.4 mg. #34KD32									
A	1,000	7.3	96.0	0.01816	17.049	29.2	16	344.1	±1.2
B	1,050	7.0	98.7	0.01743	16.901	23.3	18	341.4	±1.8
C	1,100	7.4	99.3	0.01835	17.019	15.5	17	343.6	±1.9
D	1,150	12.0	99.1	0.02984	17.014	13.9	17	343.5	±1.1
E	1,200	23.9	99.6	0.05927	16.793	40.7	18	339.4	±0.5
F	1,250	30.7	99.9	0.07617	16.680	61.4	21	337.4	±0.4
G	1,300	11.6	99.7	0.02890	16.496	29.6	22	334.0	±1.1
Total gas		100.0	99.3	0.24814	16.793	38.6	19	339.4	
(c) TEJ-3. Phlogopite. J=0.011726±0.50%. Wt.=7.9 mg. #23KD37									
A	1,000	15.1	98.3	0.1154	17.704	12.5	54	340.3	±0.8
B	1,050	9.0	98.9	0.0690	18.045	12.3	55	346.3	±0.9
C	1,100	11.4	99.0	0.0871	18.718	11.1	53	358.0	±0.8
D	1,150	18.5	993	0.1410	18.741	9.6	56	358.4	±0.6
E	1,175	14.6	99.4	0.1119	18.049	12.3	62	346.3	±0.5
F	1,200	14.6	99.5	0.1113	17.784	13.5	26	341.7	±0.5
G	1,225	11.5	99.5	0.0881	17.614	13.0	43	338.7	±0.6
H	1,250	5.3	98.7	0.0402	17.377	6.6	60	334.6	±0.9
Total gas		100.0	99.1	0.7639	18.076	11.6	50	346.8	
(d) ZOM-23. Phlogopite. J=0.011726±0.50%. Wt.=8.0 mg. #27KD37									
A	1,000	15.9	98.9	0.1435	17.684	46.4	53	339.4	±0.47
B	1,050	13.5	99.3	0.1218	17.555	24.0	63	337.7	±1.47
C	1,100	23.7	99.8	0.2138	17.537	545	68	337.4	±0.43

D	1,150	20.7	99.9	0.1862	17.420	30.0	69	335.3	±0.34
E	1,175	9.9	98.9	0.0894	17.084	13.8	65	329.4	±1.20
F	1,200	9.4	99.3	0.0852	17.180	10.2	22	331.1	±0.77
G	1,225	6.8	997	0.0616	17.199	5.3	38	331.4	±0.61
Total gas		100.0	99.5	0.9015	17.437	32.5	58	335.6	

Ages calculated assuming an initial $^{40}Ar/^{36}Ar$=295.5±0. All precision estimates are at the one-sigma level of precision. Ages of individual steps do not include error in the irradiation parameter *J*. No error is calculated for the total gas age.
(a) Isochron information: [$^{40}Ar/^{36}Ar]_i$=220±48; MSWD=0.63; steps A–G with 100% of $^{39}Ar_K$. Isochron age: 335±2.0 Ma
(b) Isochron information: [$^{40}Ar/^{36}Ar]_i$=461±97; MSWD=0.47; steps A–G with 100% of $^{39}Ar_K$. Isochron age: 338.2±3.0 Ma
(c) Isochron information: [$^{40}Ar/^{36}Ar]_i$=4,093±4,214; MSWD=0.06; steps A–G with 70.6% of $^{39}Ar_K$. Isochron age: 321.5±32.6 Ma
(d) Isochron information: [$^{40}Ar/^{36}Ar]_i$=1,329±557; MSWD=0.76; steps A–G with 100% of $^{39}Ar_K$. Isochron age: 328.1±6.3 Ma. Plateau age: 336.2±1.7 Ma with 57.9% of gas on plateau in 1,050 through 1,150 steps

igneous bodies with the migmatite foliation, the thorough mixing with migmatite at the contacts, and the location of the igneous rocks in the high-grade core of the Aracena Massif, with the metamorphic grade quickly diminishing outward (Crespo 1991). The maximum metamorphic P–T conditions for the Aracena Massif (>920 to 1,000°C; 4 to 6 kbar), identified by Patiño Douce et al. (1997) and Diaz-Azpiroz et al. (2004), are also consistent with the metamorphism being directly related to the intrusion of mafic magmas.

West of the Aracena Massif is the large synmetamorphic Beja Igneous Complex, which comprises layered olivine–hypersthene gabbro, quartz diorite, troctolite, and anorthosite and contains Fe–Ti–V oxide concentrations and Cu–(Ni) disseminations similar to those of Aguablanca and Cortegana (Mateus et al. 2001). Amphibole $^{40}Ar/^{39}Ar$ ages of ca. 352 to 338 Ma were recorded for the regional metamorphism (Dallmeyer et al. 1993). These ages overlap with those found for Aracena and Aguablanca, strengthening the idea that mafic–ultramafic magmatism, sulfide ore formation, and high-T low-P regional metamorphism were largely coeval (Fig. 10).

Geochemistry of the igneous host rocks

Representative chemical analyses of rocks from a database of fifty three samples from the Santa Olalla Plutonic Complex are shown in Table 2. Analyses were carried out at the laboratories of the Instituto Geológico y Minero de España (IGME) by XRF for major and trace elements except Na_2O that was measured by AAS. Rare earths and Y were measured by ICP-MS-TOF.

Rocks showing petrographic evidence of pervasive hydrothermal alteration or having significant sulfur content (>0.3 wt% S) were excluded from the database. For calculations, the analyses have been recalculated on a S- and water-free basis and normalized to 100 wt%; all sulfur is assumed to be in the form of pyrrhotite and, thus, an equivalent proportion of iron has been subtracted from the total sum. Complementary data can be found in Casquet et al. (2001) and in the Electronic supplementary material.

The Aguablanca Gabbronorite Unit

The less altered rocks of the Gabbronorite Unit are characterized by high silica contents (48.0–57.3 wt% SiO_2; average 52.3 wt%) but are slightly depleted in FeO_t (6.0–16.5 wt%; average 8.8 wt%) and TiO_2 (0.23–0.83 wt%; average 0.49 wt%), CaO (6.1–14.3 wt%; average 7.6 wt%), alkalis (specially Na_2O), and Al_2O_3 (7.2–17.3 wt%; average 10.8 wt%) as well as in Y, Ce, and Eu compared to average basalt (e.g., Middlemost 1985). Total REE content is low

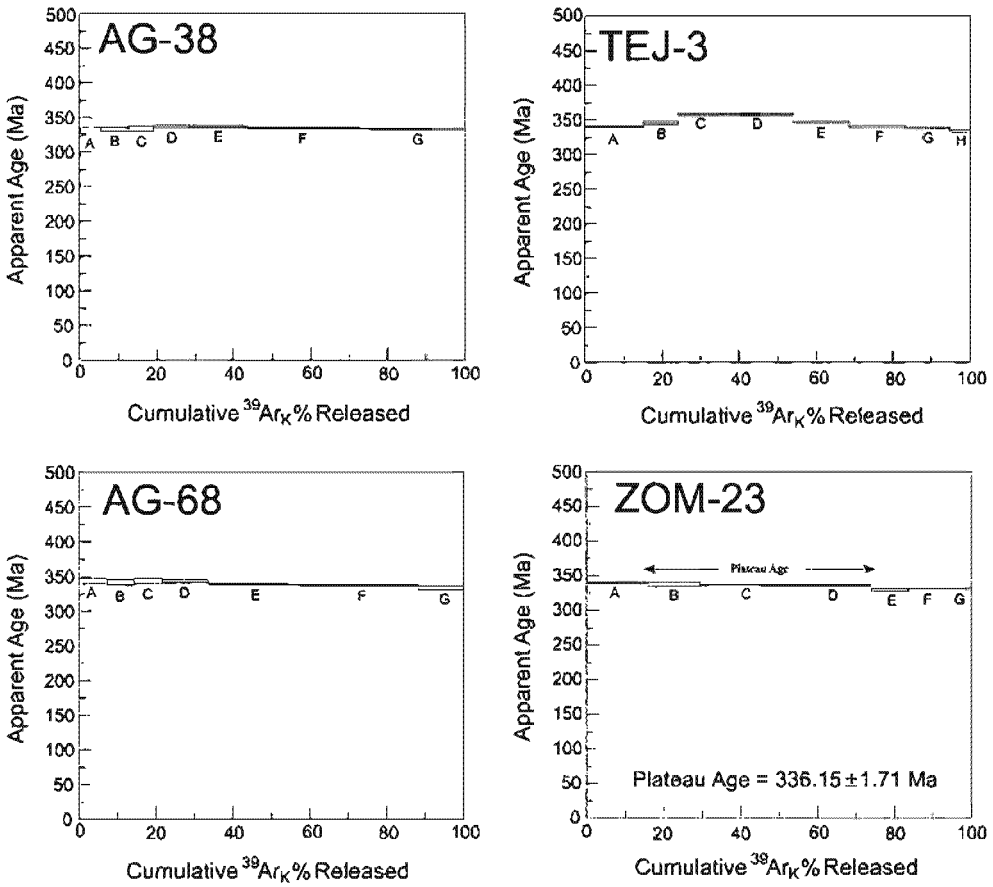

Fig. 9 ^{40}Ar–^{39}Ar age spectra diagrams for step-heating experiments of phlogopite mineral separates from the Aguablanca deposit (AG-38 and AG-68) and the Cortegana prospect (TEJ-3 and ZOM-23)

(5 57 ppm), but the rocks have relative enrichment in LREE ($[La/Sm]_{MN}$=0.53 3.1; average 2.3; $[La/Yb]_{MN}$= 0.6 7.5; average 4.1). The Mg number (Mg#, atomic Mg/ Mg+Fe) varies between 0.38 and 0.54. As a whole, the samples are broadly similar to the silica- and magnesium-rich basalt of Hoatson and Sun (2002).

Most of the rocks of the Gabbronorite Unit have geochemical features of cumulates, such as high MgO (8.3 19.1 wt%), Ni (96 927 ppm), and Cr (670 1,504 ppm) contents (Casquet et al. 2001), but cumulate textures are uncommon. The composition of the Contact Gabbro and the fact that the outcropping rocks were close to the roof of the intrusion (Casquet 1980) make it unlikely that such a geochemical pattern was controlled by in situ accumulation; more likely, it is a feature inherited from a deep source. Different explanations include: (a) a parental MgO-rich magma; (b) formation of an olivine/pyroxene cumulate and subsequent remelting; (c) major assimilation of amphibolite or dolostone; (d) plagioclase fractionation and concomitant Fe Mg enrichment; and (e) a deep stratified magma chamber. Most of these alternatives are at odds with the geochemical and geological features, and (e) is the most likely possibility, i.e., a chemical and density gradient in a magma chamber. More dense and mafic melt should accumulate in the bottom of the chamber, whereas more felsic magmas should concentrate in the upper part, as has been described by Beard and Day (1988) for the Smartville Complex, USA, or by Cawthorn and Kruger (2004) for the Mount Ayliff intrusion, South Africa.

The composition of the Contact Gabbro is probably the best approximation to the magma that formed the Gabbronorite Unit because it is interpreted to be a chilled margin without syncrystallizational modifications. Its composition is close to that of the average Gabbronorite Unit but is slightly enriched in Al_2O_3, CaO, K_2O, Rb, Sr, Ba, and U and depleted in FeO, Cr, Nb, and Y (Table 2 and Figs. 12, 13, 14 and 15).

Most of the rocks plot on linear trends on Pearce element ratio diagrams (Fig. 12). The Al/Ti vs Ca/Ti and Si/Ti vs (Fe+Mg)/Ti ratios define straight lines with good correlation, which overlap with the orthopyroxene control line as calculated from the average orthopyroxene composition in the Gabbronorite Unit. In these plots, only four samples could arguably be related to olivine fractionation. Most of the rocks belonging to the Gabbronorite Unit plot in the norite field of the CaO MgO diagram (Fig. 13), in between the tie lines of the composition of orthopyroxene and plagioclase. These geochemical trends are consistent with the petrographic observation that the Gabbronorite Unit

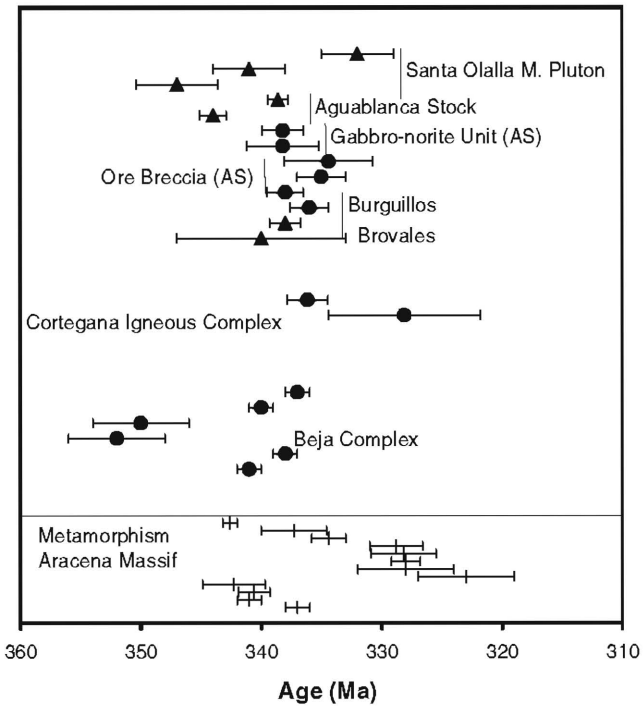

Fig. 10 U–Pb (*triangles*) and Ar–Ar ages (*circles*) of metaluminous plutonic rocks of the Ossa Morena Zone. Data from Garcia Casquero (1995), Casquet et al. (1998), Pin et al. (1999), Montero et al. (2000), Romeo et al. (2004), Spiering et al. (2005), and this study. For comparison, Ar–Ar ages of the regional metamorphism in the Aracena Massif are also included (Dallmeyer et al. 1993; Castro et al. 1999). *AS* Aguablanca Stock

always has higher proportions of orthopyroxene than clinopyroxene.

The Aguablanca Diorite Unit and the Santa Olalla Main Pluton

Rocks of the Diorite Unit and the Santa Olalla Main Pluton show neither petrographic nor chemical evidence of cumulus processes. They are geochemically different from the Gabbronorite Unit, having higher SiO_2, REE, Ba, Y, Nb, Th, Zr, Ba, V, and TiO_2 but lower Cr, Co, and MgO contents. These rocks are metaluminous with SiO_2 contents between 50 and 70 wt%, K_2O up to 4.7 wt%, and low Cr values (<280 ppm; average 173 ppm). The REE content is high, averaging 173 ppm, and the rocks are also variably enriched in LREE ($[La/Sm]_{MN}$=1.5–9.6; average 3.9; $[La/Yb]_{MN}$=3.0–29.4; average 10.5). Incompatible elements show a greater range than in the Gabbronorite Unit. The K_2O content, usually above 2 wt%, and the low FeO_t+TiO_2 contents are typical of a high-K_2O calc-alkaline magmatic trend (Fig. 14). In fact, the overall trend plots on the calc-alkaline field of the FeO/MgO–SiO_2 and FeO–Na_2O+K_2O–MgO diagrams (not shown); the TiO_2 content is below that of tholeiitic magmas.

Rocks belonging to the Diorite Unit and the Santa Olalla Main Pluton are geochemically similar, but in most binary diagrams, the compositions do not overlap, indicating that there is a compositional gap between both intrusive units. This is probably due to the different evolution within independent magma chambers.

Evidence for extensive contamination in a shallow magma chamber

Crustally contaminated mafic magmas are typically enriched in SiO_2, K_2O, Rb, Ba, Th, and LREE and usually have low TiO_2 contents (Lightfoot et al. 1990; Li et al. 2000). They tend to have high Th/Yb, La/Sm, La/Nb, Th/Nb, and La/Yb ratios reflecting the high LILE/HFSE ratio (Fig. 15), which usually correlates with high SiO_2 (Lightfoot et al. 1990; Li et al. 2000). Condie (2003) has also used the Ce/Yb, Sm/Nd, and Gd/Yb ratios to monitor crustal contamination. La/Nb >1.4, $[La/Sm]_{MN}$ >1.5, and Th/Ce >0.05 are typical of rocks with significant crustal contamination. Other variables such as the MgO, TiO_2, or Ce contents reflect the degree of fractional crystallization (Lightfoot et al. 1990; Li et al. 2000). Thus, the La/Sm ratio vs the MgO or Th/Nb can trace the role of fractional crystallization vs magma mixing or crustal contamination (e.g., Lesher et al. 2001). As can be seen in Fig. 15, the decrease in MgO due to accumulation of pyroxene and/or olivine is accompanied by an increase in La/Sm ratios, indicating that an AFC (assimilation-fractional crystallization) process is the more likely mechanism of magma evolution at Aguablanca. Furthermore, fractional crystallization alone is not consistent with the large variation in the Th/Nb and La/Sm ratios, which indicates that considerable crustal contamination occurred. The dominance of orthopyroxene and the increase of Gd/Yb with changing La/Sm (Fig. 15) exclude variable degrees of partial melting of a homogeneous melt as the dominant evolutionary mechanism. The Th/Nb ratio of rocks from the Gabbronorite Unit and the Diorite Unit–Santa Olalla Main Pluton are similar (0.03–1.73 vs 0.18–1.22) and usually well above the primitive mantle values (0.12), indicating that the proportion of contaminated material is high but variable (Fig. 15). Low Sr/Y ratios, usually less than 35, suggest that the magma equilibrated with a plagioclase-rich but garnet- and amphibole-poor reservoir, i.e., middle to upper crustal environment (Defant and Drummond 1990).

Trace element and REE spider diagrams (Pearce 1996) normalized to primitive mantle (McDonough and Sun 1995) are shown in Fig. 16. The average values for the Santa Olalla Plutonic Complex show an overall enrichment in LILE (Rb, K), Th, and LREE and are strongly depleted in more compatible Cr. The moderately incompatible elements (Ti, V, Sr, Y, Zr, Ce, and Eu) show variable enrichment

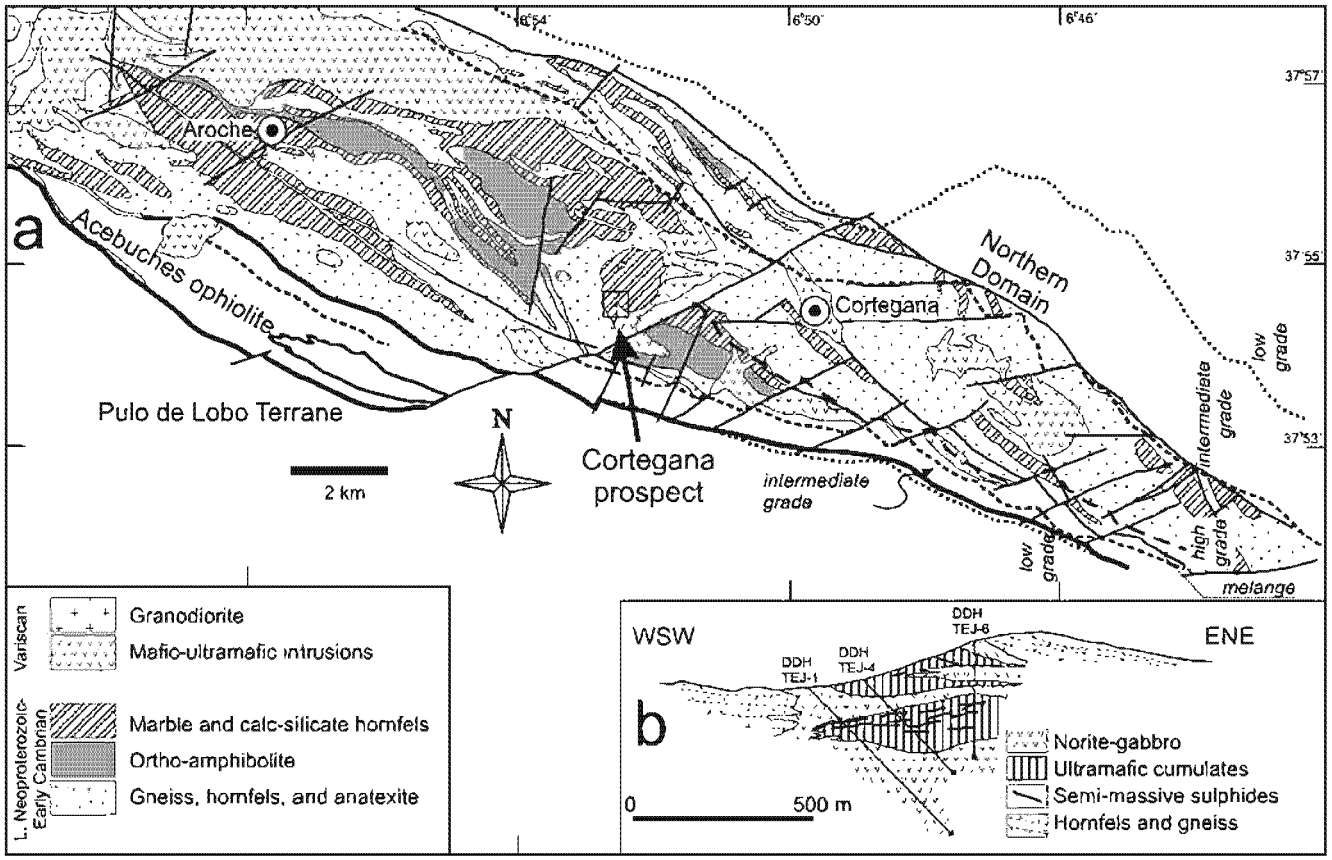

Fig. 11 Geologic setting of the central Aracena Massif showing the location of the Cortegana Igneous Complex. **a** Schematic geologic map, based on IGME (1983), with the metamorphic isograds of Crespo (1991). **b** Cross section of the Cortegana prospect based on drill-hole information of Rio Narcea Nickel (unpublished)

between 1 and 50, and Nb has a variable behavior. These values, bracketed between primitive mantle and upper continental crust (Taylor 1995), are typical of mature magmatic arcs with major crustal contamination. The ultramafic cumulates and the Gabbronorite Unit show less pronounced anomalies than the Diorite Unit and the Santa Olalla Main Pluton, which have a pattern similar to that of the middle-upper crust. A simplified binary mixing model allows to estimate that the Gabbronorite Unit has incorporated about 20 25% of crustal material, whereas the Santa Olalla Main Pluton has more than 60 80% of crustal contamination.

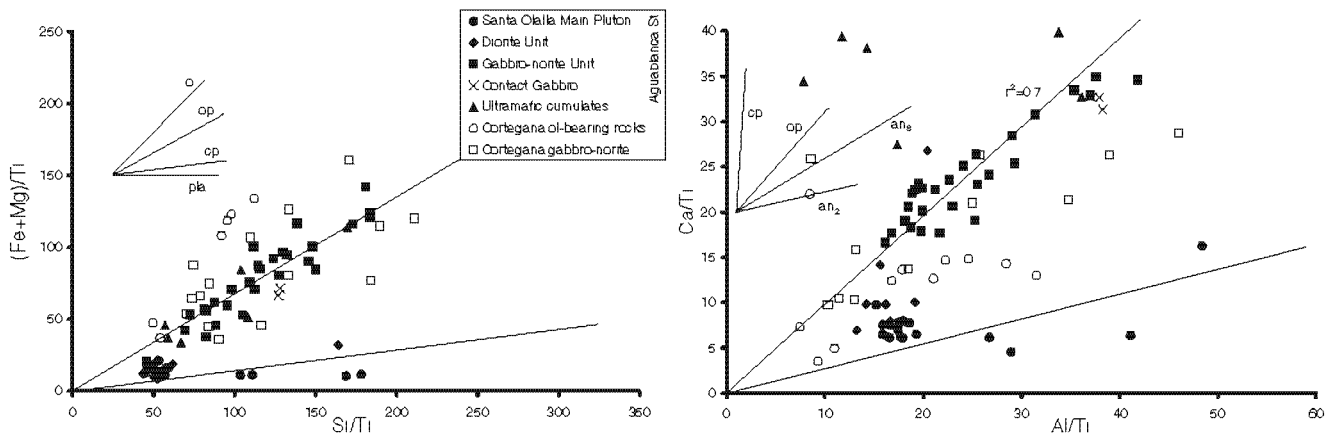

Fig. 12 Pearce element Ca/Ti vs Al/Ti and (Fe+Mg)/Ti vs Si/Ti diagrams showing that the evolution of the Santa Olalla magmatic sequence was controlled by the fractional crystallization of orthopyroxene except the more acid terms that are controlled by plagioclase. The fractionation curves of ortho- and clinopyroxene are calculated for the average composition of these minerals in the Gabbronorite Unit. Based on James et al. (2002)

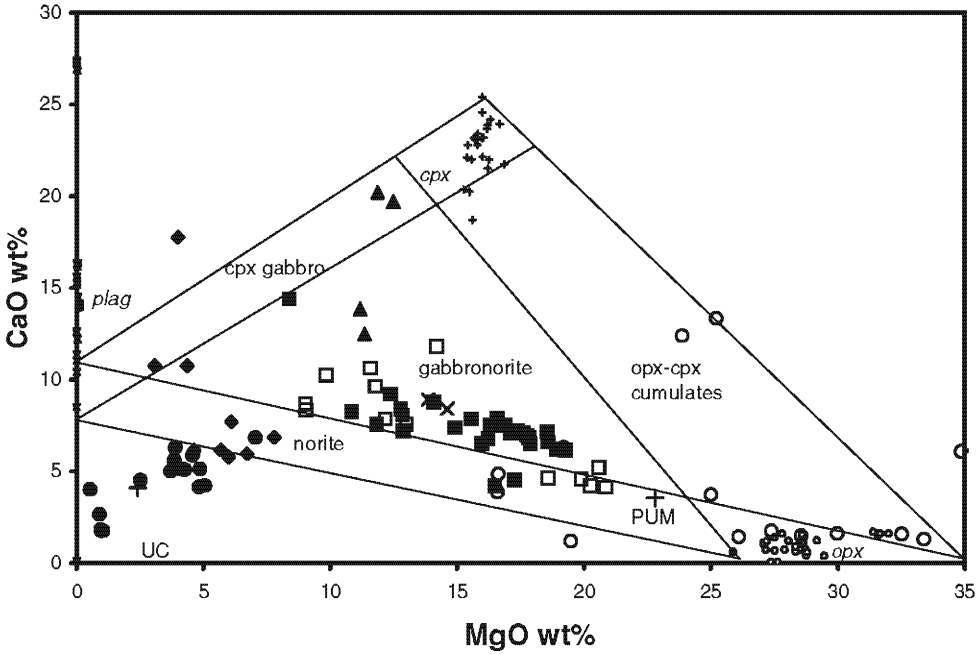

Fig. 13 CaO–MgO diagram showing the composition of the analyzed rocks. Tie lines limiting fields are only estimative. *Small x, circles*, and *crosses* represent the composition of individual plagioclase, orthopyroxene, and clinopyroxene within the Aguablanca Stock. *PUM* Average composition of the Primitive Upper Mantle, *UC* average composition of the Upper Crust. *Legend* as in Fig. 12

Rocks of the Santa Olalla Plutonic Complex are significantly enriched in REE, particularly in LREE, and have steep REE profiles with a systematic enrichment in ΣREE from the ultramafic cumulates to the Gabbronorite Unit, the Diorite Unit, and the Santa Olalla Main Pluton. This is accompanied by an increase in the LREE content, with average $[La/Yb]_{MN}$ values of 4.1 in the Gabbronorite Unit, 8.7 in the Diorite Unit, and 11.2 in the Santa Olalla Main Pluton (Fig. 16). The weak negative Eu anomaly (Eu/Eu* 0.8–0.9) and the high Sm/Nd and La/Yb ratios in the more mafic rocks are consistent with orthopyroxene fractionation and absence of plagioclase-rich cumulates. Within the Diorite Unit and the Santa Olalla Main Pluton, the negative Eu/Eu* anomaly (Eu/Eu* 0.5–0.6) is more pronounced confirming that plagioclase fractionation played a major role in the evolution of these rocks.

All rocks analyzed show evidence of contamination or accumulation and, accordingly, the chemical composition of the primitive magma cannot be inferred with certainty. The closest approximation to the MgO content of the parental magma can be estimated following the procedure of Makkonen (1996). Rare olivine (fo_{86-87}) found in the breccia fragments is interpreted as the earliest accumulated mineral. Using a K_D of 0.33 (Makkonen 1996), the magma may have been near 12 wt% MgO. Similarly, orthopyroxene compositions are consistent with olivine compositions, and the earliest orthopyroxene accumulated from parental magmas of 12 wt% MgO, with the latest orthopyroxene forming from a magma with 6.2 wt% MgO.

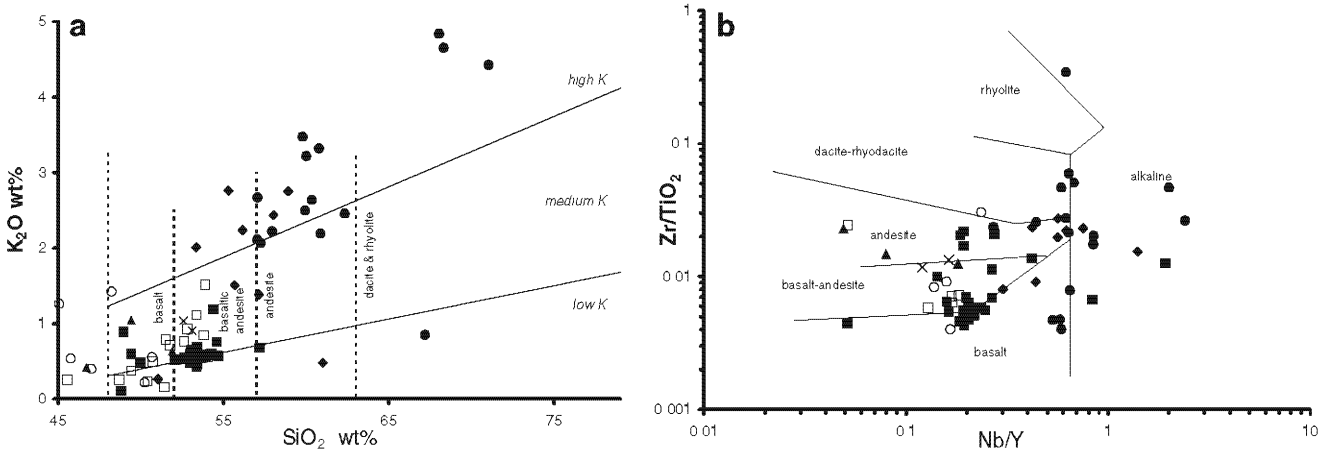

Fig. 14 Harker SiO_2–K_2O and Nb/Y vs Zr/TiO_2 (Winchester and Floyd 1977) diagrams. Note that most of the Gabbronorite Unit and the ultramafic rocks are cumulates and, thus, the chemical compositions do not correspond to the original magma. The low K_2O contents are probably due to this feature. *Legend* as in Fig. 12

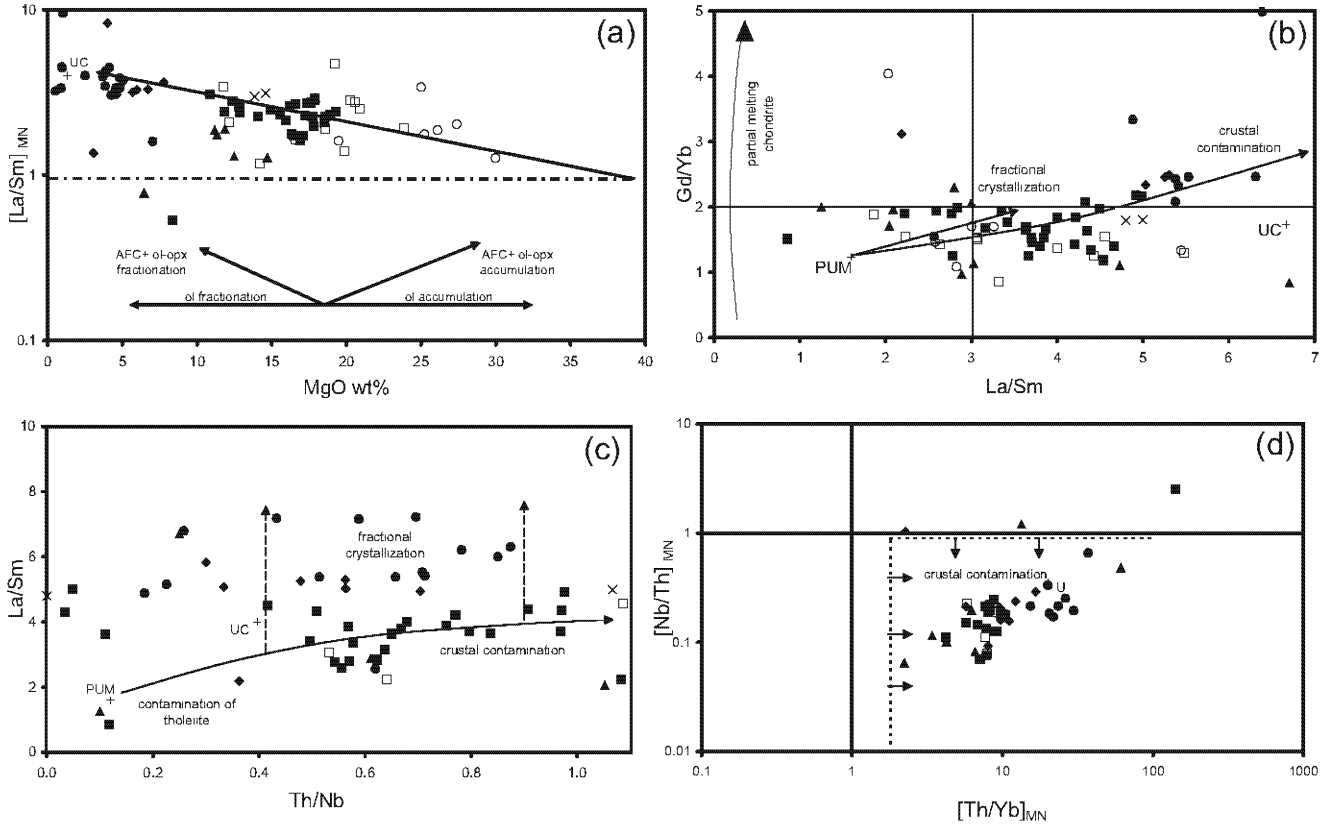

Fig. 15 Trace-element discriminant diagrams. **a** MgO% vs $[La/Sm]_{MN}$ diagram (Lesher et al. 2001). The trend is consistent with an evolution controlled by an AFC process involving fractionation pyroxene and/or olivine. **b** La/Sm vs Gd/Yb and **c** Th/Nb vs La/Sm diagrams (Lightfoot et al. 1990; Li et al. 2000). Fractional crystallization alone is not able to produce the large spread in La/Sm ratios and major crustal contamination synchronous or followed by fractional crystallization is needed to explain the variation in the La/Sm ratio. **d** $[Nb/Th]_{MN}$ vs $[Th/Yb]_{MN}$ diagram showing the estimated field for crustally contaminated magmas. The *line* represents likely minimum contamination as estimated from Condie (2003). *UC* Upper Crust as calculated from Taylor (1995) except La/Sm that is from Rudnick and Fountain (1995), *PUM* Primitive Upper Mantle as calculated from McDonough and Sun (1995). *Legend* as in Fig. 12

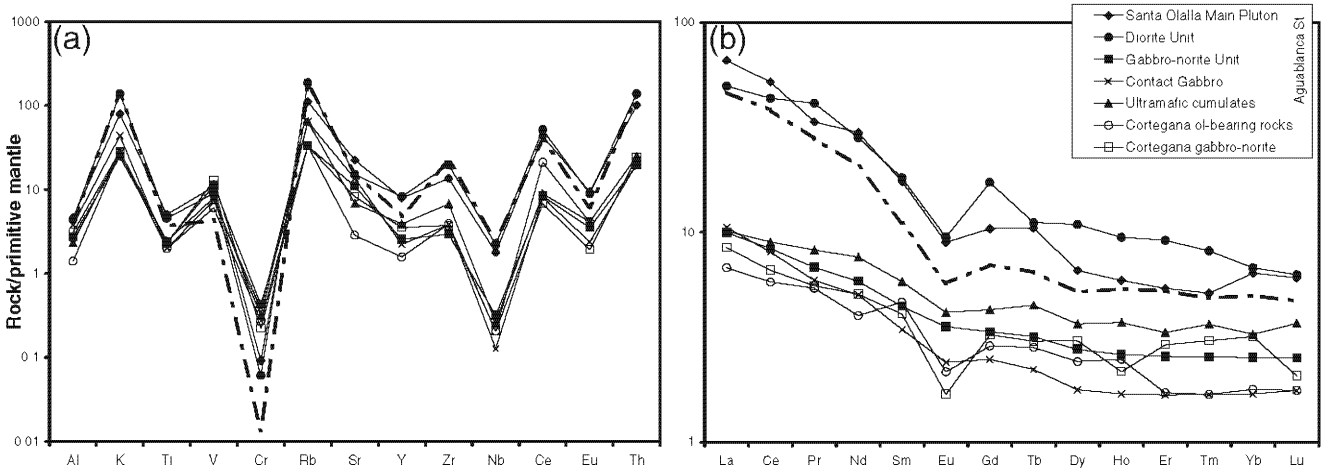

Fig. 16 Spider diagrams for more relevant elements and rare earth elements for the average values of the Santa Olalla Plutonic Complex and Cortegana Igneous Complex. Ol-bearing rocks of the Cortegana Igneous Complex include lherzolite, troctolite, harzburgite, wehrlite, and dunite. Data normalized to the Primitive Upper Mantle of McDonough and Sun (1995). The *dash-point lines* are the average values for the upper crust as calculated by Taylor (1995)

The rocks of the Cortegana Igneous Complex

Rocks of the Cortegana Igneous Complex are geochemically broadly similar to those of the Aguablanca Stock (Figs. 12, 13, 14, 15 and 16). However, the mafic rocks at Cortegana are depleted in MgO and FeO_t and enriched in CaO and K_2O with respect to Aguablanca, probably reflecting the interaction with quartz–feldspar-rich rocks. This is also reflected in the pronounced negative Eu anomaly (Eu/Eu* 0.55). Only the olivine-rich rocks are more primitive, as reflected by their low SiO_2 and Al_2O_3 contents and high Mg#.

Strontium and neodymium isotope composition

Rb–Sr and Nd–Sm isotope data were obtained from 17 whole-rock samples from the Santa Olalla Plutonic Complex and the Cortegana Igneous Complex (Table 4 and Fig. 17). Analytical methods are as in Casquet et al. (2001). In addition, 11 whole-rock Sr and Nd isotope data from the Santa Olalla Plutonic Complex by Casquet et al. (2001) were also included in the dataset. Initial Sr and Nd compositions were calculated at a reference age of 340 Ma (Table 4). Epsilon-Nd (εNd_{340}) values were calculated after Ludwig (1993).

Whole-rock $^{87}Sr/^{86}Sr_{340}$ ratios range from 0.7017 to 0.7106, and $^{143}Nd/^{144}Nd_{340}$ ratios range from 0.5118 to 0.5127. However, if one pyroxenite sample is excluded (AB-102), the ranges of Sr and Nd isotope ratios reduce significantly to 0.7059–0.7106 and 0.5118–0.5125, respectively. Values of εNd_{340} range from −8 to +9, but if the AB-102 pyroxenite is excluded, all values are negative and between −8.0 and −3.2 (Table 4).

Isotope data are best shown on $^{87}Sr/^{86}Sr_{340}$ vs Rb/Sr and $^{143}Nd/^{144}Nd_{340}$ vs Sm/Nd plots (Fig. 17a,b). This type of diagram allows the discrimination of magmatic differentiation and other processes such as crustal assimilation or magma mixing. By combining information, three groups of rocks can be distinguished.

The first group corresponds to the Santa Olalla Main Pluton and the Aguablanca Diorite Unit. The ranges of $^{87}Sr/^{86}Sr_{340}$ and $^{143}Nd/^{144}Nd_{340}$ values are small, 0.7085–0.7106 and 0.51179–0.51190, respectively. The Rb/Sr and Sm/Nd ratios of the group range from ca. 0.03 to 0.54 and ca. 0.18 to 0.23, respectively.

The second group includes the Gabbronorite Unit and most of the pyroxenite fragments from the breccia. This group is, on average, isotopically more primitive than the first group. The ranges of Sr and Nd isotope ratios are also small, 0.7065–0.7084 and 0.51187–0.51196, respectively. Pyroxenite AB-102 has the most primitive composition with an initial Sr isotope ratio of 0.70171 and an initial Nd isotope ratio of 0.51267. Rb/Sr and Sm/Nd ratios within this group are between 0.06 and 0.9, and 0.19 and 0.36, respectively.

The third group consists of the Cortegana samples. Initial Sr isotope ratios are between 0.7046 and 0.7074, i.e., generally more primitive than those of the other two groups. The initial Nd isotope ratios are between 0.51181 and 0.51204, and the Rb/Sr and Sm/Nd ratios range from 0.06 to 1.81 and 0.28 to 0.4, respectively.

Most samples have initial $^{87}Sr/^{86}Sr$ ratios higher than 0.7050 and negative εNd values, confirming that a significant proportion of continental crust has been added to a basaltic magma. Moreover, in rocks belonging to the Santa Olalla Plutonic Complex, the uniform Sr and Nd isotope ratios and the relatively large range of Rb/Sr and Sm/Nd values within each group (Fig. 17a,b) imply that magmatic variability was the result of either differentiation or mixing of isotopically similar consanguineous magmas. In the Cortegana rocks, the Sr and Nd isotope composition and the Rb/Sr and Sm/Nd values suggest mixing between isotopically different sources.

However, chemical diversification within the Gabbronorite Unit and pyroxenite cumulates probably resulted from mixing between isotopically homogeneous pyroxene cumulate and Rb-rich interstitial magma in different proportions. An increase in the ratio of groundmass/pyroxene crystals resulted in an increase of the Rb/Sr ratio which can be as high a 0.89 in pyroxenite AG-72, without modifying the Sr (and Nd) isotope composition.

Pelitic and calc-silicate rocks equivalent to those around the Aguablanca Stock have variable $^{87}Sr/^{86}Sr_{340}$ ratios, but most are between 0.7104 and 0.7119 with Rb/Sr ratios of 0.11 to 0.73 (Darbyshire et al. 1998). In Fig. 17a, pyroxenite cumulates and rocks belonging to the Gabbronorite Unit plot between these values and depleted mantle. The same holds true for the Nd isotope composition (Fig. 17b).

Figure 17c is a εSr–εNd plot that includes additional data on other metaluminous plutons from the Ossa Morena Zone. All rocks, besides the anomalous pyroxenite sample AB-102, have subchondritic εNd and superchondritic εSr values and define a classical crust–mantle mixing trend. Large-scale crustal contamination is clearly indicated for the Santa Olalla Main Pluton and Aguablanca Stock, while the Cortegana Complex displays a lower degree of crustal contamination.

The Cortegana rocks define an apparently contradictory trend of decreasing $^{87}Sr/^{86}Sr$ and $^{143}Nd/^{144}Nd$ values with increasing Rb/Sr and Sm/Nd ratios (Fig. 17a,b). One likely end member lies on the mixing line between the depleted mantle basaltic source and regional supracrustal rocks and is isotopically more juvenile than parental magmas of the Santa Olalla Main Pluton and the Aguablanca Stock. A second likely end member remains puzzling because it had higher Rb/Sr and Sm/Nd ratios. The samples closer to this

Table 4 Radiogenic isotope data of igneous rocks

		Rb (ppm)	Sr (ppm)	$^{87}Rb/^{86}Sr$	$^{87}Sr/^{86}Sr$	$^{87}Sr/^{86}Sr_{340\ Ma}$	$\varepsilon\ Sr_{340\ Ma}$	Sm (ppm)	Nd (ppm)	$^{147}Sm/^{144}Nd$	$^{143}Nd/^{144}Nd$	$^{143}Nd/^{144}Nd_{340\ Ma}$	$\varepsilon Nd_{340\ Ma}$
Aguablanca Stock													
AB-102	Pyroxenite	1.0	5.0	0.5785	0.704506	0.701707	−34	0.4	1.1	0.2199	0.513155	0.512665	+9.0
AG-72	Pyroxenite	120.0	135.0	2.5746	0.718956	0.706496	+34	0.6					
AG-207-1	Pyroxenite	56.1	153.7	1.0560	0.713354	0.708243	+59	2.7	12.0	0.1369	0.512173	0.512123	−6.5
AG-207-2	Pyroxenite	28.9	334.1	0.2504	0.709629	0.708417	+61	2.4	9.5	0.1545	0.512308	0.512279	−4.6
AG-207-4	Pyroxenite	19.6	117.6	0.4834	0.710765	0.708426	+62	4.4	20.2	0.1328	0.512163	0.512146	−6.5
AG-207-5	Pyroxenite	48.7	226.7	0.6217	0.711314	0.708305	+60	2.9	12.5	0.1399	0.512217	0.512172	−5.8
AG-97	Gabbronorite	21.6	146.3	0.4277	0.710009	0.707939	+55	2.1	8.1	0.1524	0.512236	0.511897	−6.0
AG-5	Gabbro	20.2	256.0	0.2281	0.709387	0.708283	+60	1.3	5.3	0.1440	0.512230	0.511909	−5.7
C-12	Diorite	109.4	294.2	1.0763	0.715820	0.710611	+93						
C-5	Diorite	104.8	268.2	1.1317	0.714350	0.708873	+68	5.5	27.0	0.1240	0.512160	0.511884	−6.2
Santa Olalla Main Pluton													
C-18	Q-diorite	10.8	415.5	0.0752	0.709660	0.709296	+74	22.0	99.3	0.1338	0.512149	0.511851	−6.9
AG-82	Granodiorite	128.1	359.0	1.0335	0.715559	0.710557	+92	11.3	61.6	0.1107	0.512040	0.511793	−8.0
Cortegana Complex													
TE-4	Norite	16.7	288.5	0.1675	0.708197	0.707387	+47	3.7	12.5	0.17894	0.512439	0.512040	−3.2
TEJ-7	Olivine–websterite	16.0	110.2	0.4201	0.707921	0.705888	+25	1.0	3.5	0.17272	0.512411	0.512026	−3.4
TEJ-9	Olivine–websterite	10.1	123.8	0.2360	0.707065	0.705923	+26	1.0	3.0	0.20151	0.512486	0.512037	−3.2
TEJ-11	Harzburgite							3.2	8.3	0.23307	0.512334	0.511815	−7.6
ZOM-23	Lherzolite	38.0	21.0	5.2468	0.730020	0.704626	+8	2.0	5.0	0.24181	0.512441	0.511903	−5.8

Analyses CAI Geochronology and Isotope Geochemistry, Universidad Complutense Madrid. Errors (2σ) are 0.01% (Sr) and 0.006% (Nd). Chemical analysis of the rocks in Table 2, Casquet et al. (2001), and the Electronic supplementary material

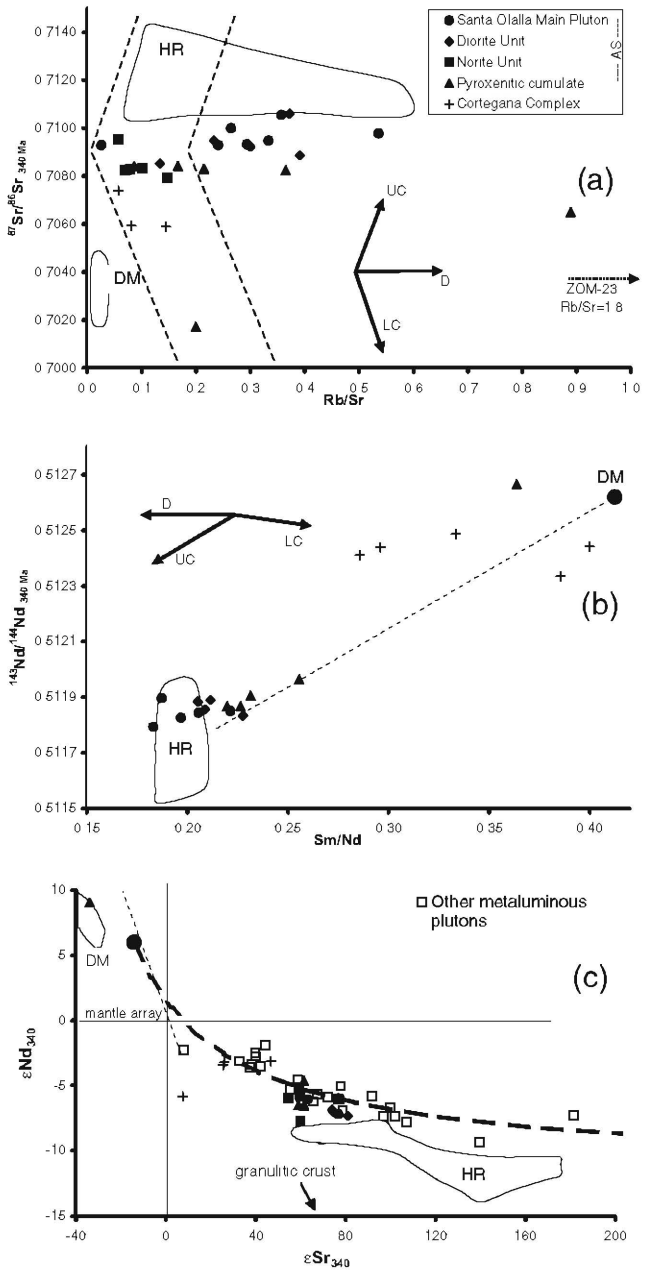

Fig. 17 Rb/Sr–$^{87}Sr/^{86}Sr$, Sm/Nd–$^{143}Nd/^{144}Nd$, and εSr–εNd plots of rocks of the Aguablanca Stock, adjacent plutonic rocks, and host rocks of late Neoproterozoic–middle Cambrian age (Galindo et al. 1995; Darbyshire et al. 1998; Casquet et al. 2001). *DM* represents the Sr and Nd isotope compositions of the average depleted mantle at the age of formation (Leeman and Dasch 1978; Fauré 1986; McDonough and Frey 1989; Workman and Hart 2005). The field HR includes the composition of the host rocks to the Santa Olalla Pluton (Galindo et al., unpublished data). *D* represents the differentiation trend with increase in plagioclase and depletion in olivine and pyroxene, while *UC* and *LC* show the likely trend of evolution during mixing with average upper crustal and lower crustal rocks, respectively. Most of the analyzed rocks plot on a mixing curve between a juvenile magma and the host metasedimentary rocks

second hypothetical end member are ZOM 23, with an $^{87}Sr/^{86}Sr_{340}$ ratio of 0.7046 and an $^{143}Nd/^{144}Nd_{340}$ of 0.51190, and TEJ 11 (not analyzed for Sr), with an $^{143}Nd/^{144}Nd340$ ratio of 0.51181. No candidates for this crustal contaminant member have been recognized so far in the area, and its geological implications remain unknown. The high Rb/Sr ratio is compatible with a granitic magma or a pelitic rock, a feature consistent with the low Nd isotope ratio (see Rollinson 1993), but the low Sr isotope ratio points toward a depleted source. High Sm/Nd values might be explained by melting reactions involving garnet. A low crustal metapelite can concentrate intermediate and heavy REE with high Sm/Nd ratios that increase with pressure (Bea et al. 1997). Thus, garnet bearing low crustal felsic continental could be a suitable source for the Cortegana mafic–ultramafic rocks second end member. Field evidence suggests that mixing between juvenile magmas and the host migmatite took place at or near the emplacement level (Fig. 4h). There are published Sr isotope composition data for the Cortegana migmatite (Castro et al. 1999) and Sr and Nd isotope data for late peraluminous leucogranite of likely deep migmatitic origin in the Olivenza-Monesterio antiform (Bachiller 1996). Only Los Molares migmatite (Rb/Sr: 7.2, $^{87}Sr/^{86}Sr_{340}$: 0.7038; Castro et al. 1999) and one leucogranite (Sample Bp2; Rb/Sr: 12, $^{87}Sr/^{86}Sr_{340}$; 0.7052, Sm/Nd=0.35, $^{143}Nd/^{144}Nd_{340}$: 0.5120; Bachiller 1996) approach the isotopic characteristics of the second end member.

Lead isotope ratios of pyrrhotite are consistent with the Nd and Sr isotope data. Four analyses range between 17.935 and 18.068 ($^{206}Pb/^{204}Pb$), 15.566 and 15.602 ($^{207}Pb/^{204}Pb$), and 38.159 and 38.252 ($^{208}Pb/^{204}Pb$) (Marcoux et al. 2002; Tornos and Chiaradia 2004). These values plot slightly below the calculated growth curve of the area (μ=9.7; Nägler 1990) that is broadly similar to the average crustal growth curve of Stacey and Kramers (1975) and well above the mantle curve (Doe and Zartman 1979). This indicates that most of the lead was derived from a rather uranogenic source, i.e., the host metasedimentary rocks. Because the average lead content of upper crustal rocks is well above that of the mantle and lower crust, minor crustal contamination of juvenile magmas can significantly modify the primary lead isotope signature. The Aguablanca Stock apparently underwent larger crustal contamination than other equivalent systems, like Voisey's Bay (Amelin et al. 2000) where the μ values are always lower than 8.0.

Discussion and genetic model

The unusual geologic setting of the Aguablanca deposit has given place to different genetic hypotheses. The earliest models suggested a magmatic stratiform mineralization

style located in a zoned pre-Variscan sill equivalent to Sudbury or Noril'sk, and then tilted to vertical position during the Variscan orogeny (Lunar et al. 1997). This hypothesis relies mainly on the comparison with other magmatic Ni Cu deposits, presumed geopetal structures found in drill core, chemical zonation (Ortega et al. 2000), and on the recognition of an isoclinally folded magmatic layering (Ortega et al. 2002). This hypothesis, however, is at odds with the more recent geochronological data that show that the Aguablanca Stock is of Variscan age (ca. 340 335 Ma) (Casquet et al. 1999, 2001; Romeo et al. 2004; Spiering et al. 2005). Moreover, structural and geological evidence indicates that the orebody consists of a discordant magmatic breccia pipe within a mafic stock (Tornos et al. 1999, 2001; Casquet et al. 2001). The combination of the available geological and geochemical data suggests that two concurrent events were involved in the development of the Aguablanca deposit (Figs. 18 and 19).

Stage I: development of a deep differentiated magma chamber

The presence of a deep magma chamber below the Aguablanca orebody was inferred by Tornos et al. (1999, 2001) and Casquet et al. (2001) and has been recently confirmed by geophysical studies (Simancas et al. 2003). Moreover, geological, geochemical, and geochronological evidence strongly suggests that the Cortegana Igneous Complex is an exhumed part of this deep igneous complex.

The magmatic variability of the Santa Olalla Plutonic Complex can be interpreted as resulting from the AFC evolution of a basaltic parental melt in a crustal magma chamber. The Gabbronorite Unit was formed by the early contamination of REE, Sr, and LILE-depleted primitive melt with more evolved material, very likely continental crust, with later fractionation of orthopyroxene. Such a process is consistent with the evolution from basalt with tholeiitic composition to calc-alkaline basalt-andesite. Further fractional crystallization of hornblende and plagioclase formed the Santa Olalla Main Pluton and the Diorite Unit of the Aguablanca Stock. The geochemical data show that contamination and fractional crystallization were synchronous but highly variable processes (Casquet et al. 2001). The geochemistry of the igneous rocks is consistent with their derivation from a stratified magma chamber. Due to density contrasts, immiscible sulfide melt would pond near the footwall along with pyroxenitic and norite-gabbro cumulates below a more evolved residual magma.

At Aguablanca, evidence for widespread crustal assimilation includes the high orthopyroxene/olivine ratio, the presence of inclusions of Al-rich minerals, the abundance of host-rock xenoliths, the enrichment in silica and incompatible elements, and the crustal isotopic signatures of Nd, Sr, S (see below), and Pb. All these features preclude magma mixing or incorporation of country rock sulfur through metamorphic devolatilization as the principal cause for sulfide immiscibility. Crustal contamination is a common feature of rocks hosting magmatic Ni (Cu) deposits such as Noril'sk (Lightfoot et al. 1990), Voisey's Bay (Amelin et al. 2000; Li and Naldrett 2000), Sudbury (Lightfoot et al. 1997a), Kalatongke (Shengao et al. 2003), or the Juva district (Makkonen 1996), as well as other layered complexes such as Bushveld (Davies et al. 1980). However, the degree of contamination seems to be much higher in Aguablanca than in many other magmatic nickel deposits. For example, at Voisey's Bay, the Th/Nb ratio is up to 0.8 (Li et al. 2000), whereas in Aguablanca, the Norite Unit has ratios up to twice as high. The compositional similarity between the Contact Gabbro and the Gabbronorite Unit shows that most

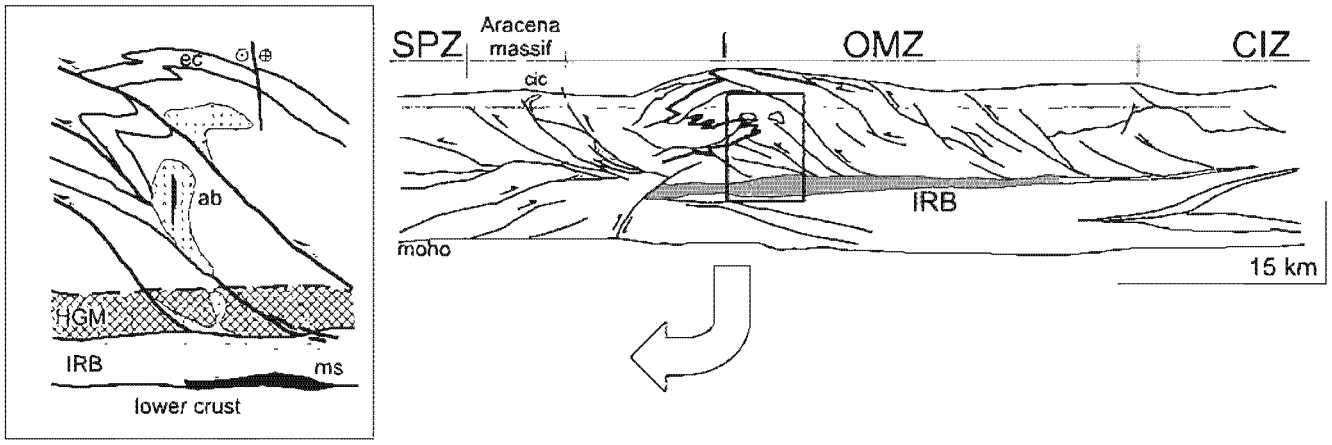

Fig. 18 Cross section of the continental crust in the Ossa Morena Zone showing the relationships between the deep-layered complex (IRB, IBERSEIS Reflective Body) with stratiform Ni–(Cu) mineralization (*ms*) and the metaluminous plutonism with Aguablanca-like ore deposits (*ab*). The Cortegana Igneous Complex (*cic*) probably corresponds to a dismembered part of the IRB body. Section based on Simancas et al. (2003) and Tornos and Casquet (2005). *c* Early–Middle Cambrian sediments, *HGM* zone of high-grade metamorphism adjacent to the deep magmatic complex, *SPZ* South Portuguese Zone, *OMZ* Ossa Morena Zone, *CIZ* Central Iberian Zone

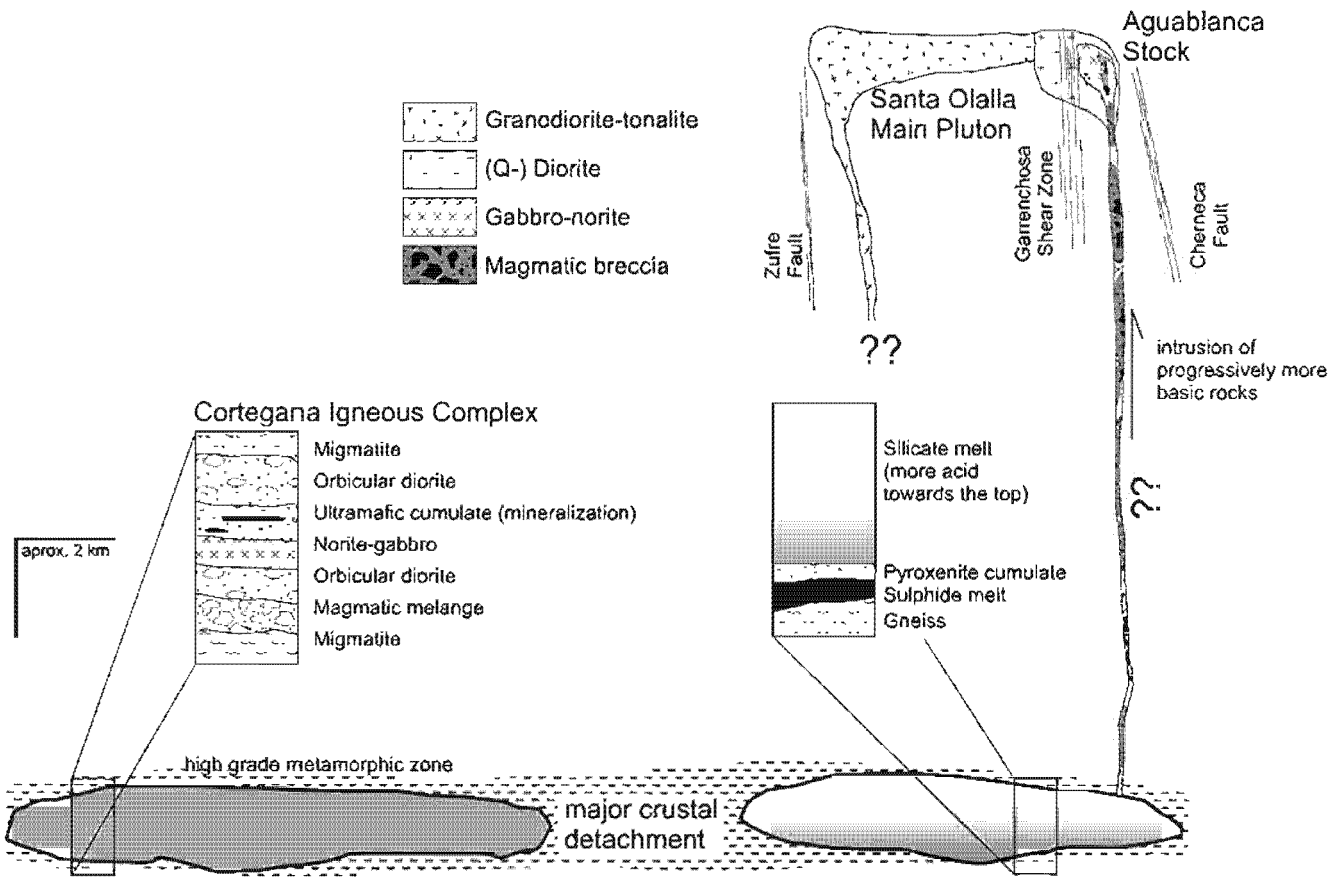

Fig. 19 Proposed genetic model for the Ni–(Cu) magmatic deposits of the Ossa Morena, including the autochthonous Cortegana prospect, the allochthonous Aguablanca orebody, and a hypothetical stratiform mineralization that forms the protore of the Aguablanca deposit

AFC processes took place at depth before the emplacement of the Aguablanca Stock.

The most likely candidate for the crustal end member contaminant is the Late Neoproterozoic to Middle Cambrian siliciclastic sequence that forms the bulk of the Aracena Massif and dominates the basement of the Ossa Morena Zone. In fact, in the Olivenza-Monesterio area, Late Neoproterozoic slate with 0.1 2 wt% sulfur (Nägler 1990; Schäfer 1990, and unpublished data) hosts abundant small stratabound concentrations of chalcopyrite and bornite with traces of gold (Tornos et al. 2004). The relatively high Cu and Au contents of the Aguablanca ore could well be due to the assimilation of larger amounts of such a crustal component.

Contamination was an early process that took place before the crystallization of olivine, leading to early orthopyroxene crystallization and inhibiting the formation of major peridotite. This contamination did not take place in the magmatic conduits, as has been suggested for Voisey's Bay or Noril'sk (Li et al. 2000, 2001), but rather in a deep-seated magma chamber as proposed for Noril'sk by Lightfoot and Keays (2005). Textural evidence indicates that sulfide immiscibility was synchronous with orthopyroxene and always before clinopyroxene crystallization.

The homogeneous sulfur isotope values of the Aguablanca ore, from +7.1 to +7.8‰ (Casquet et al. 2001), point toward a homogeneous sulfur composition during the ore-forming process. Mass balance considerations assuming that $\delta^{34}S$ of the uncontaminated primitive magmas was between −3 to +2‰ and that of the country rocks was 14 21‰ (Tornos and Velasco 2002) suggest that up to 30% of the sulfur was of external derivation to the magma.

The depth of the magma chamber at ca. 340 Ma was between 12 and 19 km, as estimated from the present depth of the IRB body plus the inferred depth of intrusion of the Aguablanca Stock (Casquet 1980). Pressure estimates obtained from mineral equilibria geobarometry in the Gabbronorite Unit (4.3 5.7 kbar) record pressures that probably correspond to those of the deep magmatic complex and agree with the depth estimation above. These values are consistent with the lithostatic pressure of about 4 6 kbar, i.e., 12 18 km depth, obtained by Patiño Douce et al. (1997) and Díaz-Azpiroz et al. (2004) for the Aracena metamorphism.

The geology of the Aracena Massif and the geophysical data (Simancas et al. 2003) show that the deep magmatic complex is highly discontinuous and composed of several

tens of subhorizontal sills and irregular intrusions that likely evolved differently depending on the size, nature of the host rocks, temperature of intrusion, and degree of assimilation. This is consistent with the differences between the Santa Olalla Plutonic Complex and the Cortegana Igneous Complex that suggest that rocks cropping out in the Cortegana Complex are not exact equivalents to the deep intrusion underlying Aguablanca. Below Aguablanca, the intrusion of a voluminous batch of mafic magma into middle to upper crust was able to digest significant amounts of sedimentary wallrocks. The high surface ratio would favor wallrock–magma interaction and immiscibility of a sulfide melt from the parental silicate magma. The fine grain size suggests quick crystallization of pyroxene. However, at Cortegana, the presence of coarse-grained olivine and pyroxene-bearing heterogeneous rocks with abundant remnants of partially digested host rock suggests that assimilation was less effective. In fact, only sporadic sulfide blebs are found. Four $\delta^{34}S$ determinations from Cortegana yielded values of −0.1, +0.4, +2.4, and +3.1‰. These values are significantly more heterogeneous and depleted in ^{34}S than those of Aguablanca and consistent with a lower degree of contamination, a different source for sulfur or less efficient homogenization of sulfur from different sources.

Metaluminous magmatism in the Ossa Morena Zone took place in between 350 and 330 Ma, a short time span if compared with the Variscan subduction and collision that probably took place between the Early Devonian and the Late Carboniferous (ca. 416–300 Ma; Eguíluz et al. 2000). This suggests that metaluminous magmatism was not directly controlled by subduction and, instead, related with the large-scale intrusion of the deep magmatic complex into the middle crust. This deep magmatic complex was interpreted as being emplaced during a short extensional stage in the development of the subduction-related magmatic arc (Simancas et al. 2003). However, the structural relationships of the Santa Olalla Plutonic Complex strongly suggest that it was intruded during a compressional stage and favored by crustal delamination induced by left-lateral transpressional deformation (Tornos and Casquet 2005).

Stage II: upwelling and final emplacement

The emplacement of the Aguablanca Stock took place in a small subvertical pull-apart structure. Such small dilational structures can effectively focus overpressured magmas and fluids to shallow depths (Saint Blanquat et al. 1998; Sanderson and Zhang 1999). Recently, Tornos and Casquet (2005) have suggested that magma tapping from the deep-seated magma chamber took place along structures rooted in the deep magmatic complex. This model implies ascent of sulfide melt for a distance of between 8.5 and 17 km. Ascent of such dense magma is difficult to envisage unless it is assumed that small extensional structures within transpressional settings can channelize small amounts of overpressured dense magmas. In any case, only a small proportion of the total generated sulfide melt should arrive to the surface, and the existence of other magma chambers at intermediate depth is likely. Such staging chambers have been described as critical in the shallow emplacement of magmas (e.g., Jahoda et al. 1989; Saint Blanquat et al. 1998), in mesothermal gold deposits (Roberts et al. 1991; Matthai et al. 1995), in epithermal gold (Tosdal and Nutt 1998), in volcanic- and shale-hosted massive sulfide deposits (Gauthier et al. 1994), and in porphyry copper districts (Unrug et al. 1999), but there are few evidences that they controlled the formation of Ni–Cu sulfide deposits.

The foliation within the Santa Olalla Plutonic Complex suggests that there were two major feeder zones (Fig. 2). One is marked by the breccia pipes, which probably intruded both the Diorite and Gabbronorite Units. However, the foliation suggests the existence of another independent feeder zone located southward, below the Santa Olalla Main Pluton, and near the Zufre Fault. If that holds true, the Aguablanca Stock and the Santa Olalla Main Pluton represent cogenetic and broadly synchronous intrusions but developed from different feeder zones and magma chambers.

At Aguablanca, the crosscutting relationships and the orientation of the magmatic foliation suggest that successive melt batches were brought to the near surface. Available data suggest that the first magma to be tapped was the Gabbronorite Unit, immediately followed by the emplacement of the breccia pipe. The Diorite Unit, hypothetically derived from the uppermost part of the magma chamber, was probably the youngest phase. This overall intrusion scheme is broadly similar to that proposed by Beard and Day (1988) for the Smartville Complex (Northern California), where they describe the emplacement of a zoned pluton as due to the episodic intrusion of magma derived from an inferred stratified magma chamber, where differentiation and fractional crystallization took place.

Pyroxenite dominates in the breccia fragments, indicating that it probably occurred as an already crystallized cumulate in the bottom of the magma chamber but perhaps underlain by a dense sulfide melt. Overpressuring and rock failure disrupted the chamber, driving the cumulates, host rock fragments, and sulfides upward. Due to its lower viscosity, the sulfide melt could effectively separate from the silicate system and squeeze upward, concentrating in large massive sulfide blebs and in the cement of the more internal zones of the breccia, which forcefully ascended to the present position with the sulfide melt acting as a lubricant. In this context, the barren breccia and the disseminated and patchy ores probably represent the product of turbulent and variable mixing between the gabbro–noritic magma, the already crystallized cumulates, host rocks, and the sulfide melt.

Many of the Variscan metaluminous intrusions of the Ossa Morena Zone, particularly in the Olivenza-Monesterio antiform, are similar to the Aguablanca Stock. They are dominantly composed of intermediate to mafic rocks and have different types of cumulates. What seems to make Aguablanca different is the degree of crustal contamination. For example, the large Burguillos Plutonic Complex consists of a core of layered cumulates (olivine-rich harzburgite, lherzolite, olivine-bearing websterite, and melanogabbro–norite) and two outer units of diorite and tonalite composition, respectively (Pons 1982; Garcia Casquero 1995; Casquet and Galindo 2004). The Sr isotope composition at the crystallization age of 338 Ma (Dallmeyer et al. 1995; Casquet et al. 1998) ranges from 0.7047 to 0.7069. The initial εNd isotope composition is in the range of −2.4 to −3.7 (Casquet and Galindo 2004). These values are more primitive than those of the Santa Olalla Plutonic Complex and suggest a smaller degree of contamination by continental crust for the Burguillos magmas.

The Aguablanca deposit is probably the largest of a group of numerous but small synorogenic Ni–(Cu) deposits that occur in Phanerozoic arcs (Caledonides, Appalachians, North-western Cordillera, and Lachlan belt) and include Las Aguilas, Argentina (Skirrow and Sims 1999), Vakkerlien, Norway (Thompson et al. 1980), Moxie, USA (Thompson 1984), the Juva district in Finland (Makkonen 1996; Papunen 2003) or Kalatongke, China (Shengao et al. 2003), but these are only locally related with large breccia pipes (Giant Mascot, Canada; Metcalfe and McClaren 2003). The major difference of Aguablanca with these deposits is the degree of crustal contamination that seems to be much more important in Aguablanca. Probably, the unusual magmatotectonic setting and the intrusion of a large mafic body high into the crust favored abnormal crustal contamination and sulfide immiscibility.

Conclusions

The Aguablanca Ni–(Cu) deposit is related to a magmatic breccia pipe hosted by a small epizonal mafic stock that is part of a large metaluminous calc-alkaline igneous province of Variscan age dated at ca. 350–330 Ma. The deposit is interpreted as having formed in a two-stage process, which included: (a) early intrusion of a primitive tholeiitic magma along a major subhorizontal discontinuity at midcrustal depths, which evolved into a layered mafic–ultramafic complex through AFC processes; and (b) subsequent rise of magmas along small transcrustal dilational structures to upper crustal levels. Geologic relationships, Ar–Ar geochronology, and radiogenic isotope geochemistry demonstrate that part of that deep magmatic complex presently crops out in the southernmost Ossa Morena Zone (Cortegana Igneous Complex).

There is strong evidence for major contamination of the basaltic magma by sulfide-bearing crustal rocks, as traced by systematic enrichment in SiO_2 and incompatible elements, increase in $^{87}Sr/^{86}Sr$ and depletion in $^{143}Nd/^{144}Nd$ ratios, and crustal $\delta^{34}S$ and Pb isotope signatures. These data are consistent with the predominance of orthopyroxene instead of olivine in cumulate rocks and the presence of host-rock xenoliths within the intrusion. The degree of crustal contamination was probably significantly larger than in many other equivalent systems. Magma–crust interaction and immiscibility of a sulfide-rich melt were early processes and promoted by the style of intrusion in the middle crust dominated by the injection of abundant but small sills and the formation of a superheated zone. Melt stratification took place within the magma chamber and was responsible for the zonation of the Aguablanca Stock and cumulate-like geochemistry of the more mafic rocks. Comparison between the orebodies at Aguablanca and Cortegana strongly suggests that the degree and mode of crust–magma interaction was critical for mineralization. Small and/or cool intrusions were not able to effectively digest the host rock, promoting only minor mineralization. However, superheated intrusions facilitated the assimilation of large amounts of crustal material and effective homogenization, probably in a highly dynamic magma chamber.

The data presented in this study confirm that economic Ni–(Cu) sulfide deposits can form in calc-alkaline complexes developed in active-margin settings. The formation of the Aguablanca deposit required the confluence of three factors: (1) development of a deep magmatic complex with major assimilation of host rocks, (2) existence of transcrustal channelways to the upper crust, and (3) overpressured ascent of sulfide-silicate melt to a shallow emplacement level. Superposition of these processes seems to be rare and probably explains why this style of mineralization is so unusual.

The above model implies that dense sulfide melts can travel from deep midcrustal to shallow environments if the appropriate geodynamic context favors such reinjection.

Acknowledgments This study has been funded by the Spanish DGI-FEDER project BTE2003-290 and the IGME project 2004012 in the framework of the GEODE project (European Science Foundation). We acknowledge PRESUR and Rio Narcea, particularly José Luis Canto and Manuel Mesa, for facilitating the access to the mine properties and for logging drill core. A.I. would like to thank Mick Kunk from the USGS Argon Thermochronology Lab in Denver for helping and supervising the Ar–Ar geochronology and Rebecca Morris for the careful mica separation. We also would like to thank Angel Canales, Carmen Conde, Lorena Luceño, Casimiro Maldonado, Diego Morata, and David Sigüenza as well as the Department of Geology of the Aguablanca Mine for their help in the interpretation of this deposit and related ones in the Ossa Morena Zone, as well as Daniel Layton Matthews and David Lentz for the critical reviews of an early version of this work. The manuscript has

been critically reviewed by Joaquín Proenza, John Thompson, Reid Keays, and, especially, Bernd Lehmann who helped to significantly improve and clarify the original text.

References

Alexander EC, Mickelson GM, Lanphere MA (1978) Mmhb-1: a new $^{40}Ar/^{39}Ar$ dating standard. In: Zartman RE (ed) Short papers of the Fourth International Conference, Geochronology, Cosmochronology, and Isotope Geology, vol 78-701, pp 6-81

Amelin Y, Li C, Valeyev O, Naldrett AJ (2000) Nd–Pb–Sr isotope systematics of crustal assimilation in the Voisey's Bay and Mushuau intrusions, Labrador, Canada. Econ Geol 95:815–830

Arnold RG (1969) Pyrrhotite phase relations below 304°C. Econ Geol 64:405–419

Bachiller N (1996) Las alteraciones hidrotermales de los leucogranitos del Complejo intrusivo de Burguillos del Cerro (Badajoz). Edad, geoquímica y modelo de procedencia y evolución de los fluidos. Master Thesis, Universidad Complutense de Madrid, Madrid

Barnes SJ, Tang Z (1999) Chrome spinels from the Jinchuan Ni–Cu sulfide deposit, Gansu province, People's Republic of China. Econ Geol 94:343–356

Bateman R, Martin MP, Castro A (1992) Mixing of cordierite granitoid and pyroxene gabbro, and fractionation, in the Santa Olalla tonalite (Andalucia). Lithos 28:111–131

Bateman R, Rosa JD, de la Castro A (1994) Mineral chemical disequilibrium and hybridization in the Santa Olalla Pluton, Spain. Bol Soc Esp Mineral 17:83–84

Bea F, Montero P, Garuti G, Zaccarini F (1997) Pressure-dependence of rare earth element distribution in amphibolite- and granulite-grade garnets. A LA-ICP-MS study. Geostand Newsl 21:253–270

Beard JS, Day HW (1988) Petrology and emplacement of reversely zoned gabbro–diorite plutons in the Smartville Complex, Northern California. J Petrol 29:965–995

Bertrand P, Mercier JC (1985) The mutual solubility of coexisting ortho- and clinopyroxene: toward the absolute geothermometer for the natural system? Earth Planet Sci Lett 76:109–122

Bomati O, Ortega L, Lunar R, Sierra J, Moreno T, Garcia Palomero F (1999) Distribución de sulfuros de N–Cu–Fe y de minerales del grupo del platino en la mineralización intramagmática de Aguablanca (Badajoz): Implicaciones genéticas. Bol Soc Esp Mineral 22-A:19–20

Carbonell R, Simancas F, Juhlin C, Pous J, Pérez Estaún A, Gonzalez Lodeiro F, Muñoz G, Heise W, Ayarza P (2004) Geophysical evidence of a mantle-derived intrusion in SW Iberia. Geophys Res Lett 31:L11601–L11604

Casquet C (1980) Fenómenos de endomorfismo, metamorfismo y metasomatismo en los mármoles de la Rivera de Cala (Sierra Morena). Doctoral thesis, Universidad Complutense, Madrid, p 295

Casquet C (1982) Metamorfismo de contacto en el borde N del plutón de Santa Olalla de Cala con especial enfasis en las rocas carbonatadas. Rev R Acad Cienc Exactas Fis Nat Madr 76:334–363

Casquet C, Galindo C (2004) El magmatismo Varisco de la Zona de Ossa Morena. In: Geología de España, Vera JA (eds) Sociedad Geológica España-Instituto Geológico y Minero de España, Madrid, pp 194–199

Casquet C, Velasco F (1978) Contribución a la geología de los skarns cálcicos en torno a Santa Olalla de Cala (Huelva-Badajoz). Estud Geol 34:399–405

Casquet C, Galindo C, Darbyshire DPF, Noble SR, Tornos F (1998) Fe–U–REE mineralization at Mina Monchi, Burguillos del Cerro, Spain: age and isotope (U–Pb, Rb–Sr and Sm–Nd) constraints on the evolution of the ores. Abstracts GAC-MAC-APGGQ, Quebec, p A28

Casquet C, Eguiluz L, Galindo C, Tornos F, Velasco F (1999) The Aguablanca Cu–Ni (PGE) intraplutonic ore deposit (Extremadura, Spain). Isotope (Sr, Nd, S) constraints on the source and evolution of magmas and sulfides. Geogaceta 24:71–74

Casquet C, Galindo C, Tornos F, Velasco F (2001) The Aguablanca Cu–Ni ore deposit (Extremadura, Spain), a case of synorogenic orthomagmatic mineralization: isotope composition of magmas (Sr, Nd) and ore (S). Ore Geol Rev 18:237–250

Castro A, Fernandez C, El Hmidi H, El Biad M, Diaz M, Rosa J, Stuart F (1999) Age constraints to the relationships between magmatism, metamorphism and tectonism in the Aracena metamorphic belt, southern Spain. Geol Rundsch 88:26–37

Cawthorn RG, Kruger FJ (2004) Petrology and Ni–Cu–PGE potential of the Insizwa Lobe, Mount Ayliff Intrusion, South Africa. Can Mineral 42:303–324

Chai G, Naldrett AJ (1992) Characteristics of Ni–Cu–PGE mineralization and genesis of the Jinchuan Deposit, Northwest China. Econ Geol 87:1475–1495

Condie KC (2003) Incompatible element ratios in oceanic basalts and komatiites: tracking deep mantle sources and continental growth rates with time. Geochem Geophys Geosyst 4:1–28

Crespo A (1991) Evolución geotectónica del contacto entre la Zona de Ossa Morena y la Zona Surportuguesa en las Sierras de Aracena y Aroche (Macizo Iberico Meridional): un contacto mayor en la Cadena Hercinica Europea. Ediciones Universidad Granada, Granada, p 327

Czamanske GK, Kunilov VE, Zientek ML, Cabri LJ, Likhachev AP, Calk LC, Oscarson RL (1992) A proton microprobe study of magmatic sulfide ores from the Noril'sk-Talnakh district, Siberia. Can Mineral 30:249–287

Dallmeyer RD, Fonseca PE, Quesada C, Ribeiro A (1993) $^{40}Ar/^{39}Ar$ mineral age constraints for the tectonothermal evolution of a Variscan Suture in SW Iberia. Tectonophysics 222:177–194

Dallmeyer RD, Garcia Casquero JL, Quesada C (1995) $^{40}Ar/^{39}Ar$ mineral age constraints on the emplacement of the Burguillos del Cerro Igneous Complex (Ossa Morena Zone, SW Spain). Bol Geol Min 106:203–214

Dalrymple GB, Alexander EC, Lanphere MA, Kraker GP (1981) Irradiation of samples for $^{40}Ar/^{39}Ar$ dating using the Geological Survey TRIGA reactor. U.S. Geological Survey Professional Paper 1176, p 55

Darbyshire DPF, Tornos F, Galindo C, Casquet C (1998) Sm–Nd and Rb–Sr constraints on the age and origin of magnetite mineralization in the Jerez de los Caballeros iron district of Extremadura, SW Spain. Chin Sci Bull (Suppl) 43:28

Davies G, Cawthorn RG, Barton JM Jr, Morton M (1980) Parental magma to the Bushveld Complex. Nature 287:33–35

Defant MJ, Drummond MS (1990) Derivation of some modern arc magmas by melting of young subducted lithosphere. Nature 347:662–665

Diaz Azpiroz M, Castro A, Fernández C, López S, Fernández Caliani JC, Moreno-Ventas I (2004) The contact between the Ossa Morena and the South Portuguese zones. Characteristics and significance of the Aracena metamorphic belt, in its central sector between Aroche and Aracena (Huelva). J Iber Geol 30:23–52

Doe BR, Zartman RE (1979) Plumbotectonics, the phanerozoic. In: Barnes HL (ed) Geochemistry of hydrothermal ore deposits, 2nd edn. Wiley, New York, pp 22–70

Ebel DS, Naldrett AJ (1996) Fractional crystallization of sulfide ore liquids at high temperature. Econ Geol 91:607–621

Eguiluz L, Carracedo M, Apalategui O (1989) Stock de Santa Olalla de Cala (Zona de Ossa Morena, España). Stud Geol Salmant 4:145–157

Eguiluz L, Gil Ibarguchi JI, Abalos B, Apraiz A (2000) Superposed Hercynian and Cadomian orogenic cycles in the Ossa Morena

Zone and related areas of the Iberian Massif. Geol Soc Amer Bull 112:1398–1413
Fauré G (1986) Principles of isotope geology, 2nd edn. Wiley, New York, p 589
Galindo C, Darbyshire F, Tornos F, Casquet C, Cuervo S (1995) Sm-Nd geochemistry and dating of magnetites: A case study from an Fe district in the SW of Spain. In: Pasava J, Kribek B, Zak K (eds) Mineral Deposits: from their origin to environmental impacts, vol. Balkema, Rotterdam, pp 41–43
Galindo C, Casquet C (2004) El magmatismo Pre-varisco de la Zona de Ossa Morena. In: Vera JA (ed) Geología de España. SGE/IGME, Madrid, pp 190–194
García Casquero JL (1995) Intrusión múltiple y cuerpos ígneos polítípicos: El Complejo Igneo de Burguillos del Cerro, un macizo diorítico zonado en el basamento varisco de la Península Ibérica. Bol Geol Min 106:379–398
Gauthier M, Chartrand F, Trottier J (1994) Metallogenic epochs and metallogenic provinces of the Estrie-Beauce region, Southern Quebec Appalachians. Econ Geol 89:1322–1360
Giese U, Walter R, Winterfeld C (1994) Geology of the southwestern Iberian Meseta II. The Aracena Metamorphic Belt between Almonaster La Real and Valdelarco, Huelva province (SW Spain). Neues Jahrb Geol Palaontol Abh 192:333–360
Hoatson DM, Sun SS (2002) Archean layered mafic–ultramafic intrusions in the West Pilbara Craton, Western Australia: a synthesis of some of the oldest orthomagmatic mineralizing systems in the world. Econ Geol 97:847–872
IGME (1983) Mapa Geológico de España, hoja 916, Aroche. Instituto Geológico y Minero de España, Madrid, p 53
ITGE (1990) Mapa Geológico de España a escala 1/50.000 núm. 918 (Santa Olalla de Cala). Instituto Tecnológico Geominero de España, Madrid, p 46
Jahoda R, Andrews JR, Foster RP (1989) Structural controls of Monterroso and other gold deposits in NW Spain—fractures, jogs and hot jogs. Trans Inst Min Metall 98:b1–b6
James RS, Easton RM, Peck DC, Hrominchuk JL (2002) The East Bull Lake intrusive suite: remnants of a ~2.48 Ga large igneous and metallogenic province in the Sudbury area of the Canadian Shield. Econ Geol 97:1577–1606
Kerr A, Ryan B (2000) Threading the eye of the needle: lessons from the search for another Voisey's Bay in Labrador, Canada. Econ Geol 95:725–748
Kunk MJ, Winick JA, Stanley JO (2001) $^{40}Ar/^{39}Ar$ age-spectrum and laser fusion data for volcanic rocks in west central Colorado. U.S. Geological Survey Open-File Report 01-472, pp 1–94
Leeman WP, Dasch EJ (1978) Strontium, lead and oxygen isotopic investigation of the Skaergard intrusion, east Greenland. Earth Planet Sci Lett 41:47–59
Lesher CM, Burnham OM, Keays RR, Barnes SJ, Hulbert L (2001) Trace element geochemistry and petrogenesis of barren and ore-associated komatiites. Can Mineral 39:673–696
Li C, Naldrett AJ (2000) Melting reactions of gneissic inclusions with enclosing magma at Voisey's Bay, Labrador, Canada: implications with respect to ore genesis. Econ Geol 95:801–814
Li C, Lightfoot PC, Amelin Y, Naldrett AJ (2000) Contrasting petrological and geochemical relationships in the Voisey's Bay and Mushuau intrusions, Labrador, Canada: implications for ore genesis. Econ Geol 95:771–799
Li C, Naldrett AJ, Ripley EM (2001) Critical factors for the formation of a nickel-copper deposit in an evolved magma system: lessons from a comparison of the Pants Lake and the Voisey's Bay sulfide occurrences in Labrador, Canada. Miner Depos 36:85–92
Lightfoot PC, Keays RR (2005) Siderophile and chalcophile metal variations in flood basalts from the Siberian Trap, Noril'sk Region: implications for the origin of the Ni–Cu–PGE sulfide ores. Econ Geol 100:439–462
Lightfoot PC, Naldrett AJ, Gorbachev NS, Doherty W, Fedorenko VA (1990) Geochemistry of the Siberian Trap of the Noril'sk area, USSR, with implications for the relative contributions of crust and mantle to flood basalt magmatism. Contrib Mineral Petrol 104:631–644
Lightfoot PC, Keays RR, Morrison GG, Bite A, Farrell KP (1997a) Geochemical relationships in the Sudbury igneous complex: origin of the main mass and offset dykes. Econ Geol 92: 289–307
Lightfoot PC, Keays RR, Morrison GG, Bite A, Farrell KP (1997b) Geologic and geochemical relationships between the contact sublayer, inclusions and the main mass of the sudbury igneous complex: a case study of the whistle mine embayment. Econ Geol 92:647–673
Ludwig KR (1993) ISOPLOT: a plotting and regression program for radiogenic isotope data. Version 2.82. USGS Open File Report 91-445, pp 1–45
Lunar R, Garcia Palomero F, Ortega L, Sierra J, Moreno T, Prichard H (1997) Ni–Cu–(PGM) mineralization associated with mafic and ultramafic rocks: the recently discovered Aguablanca ore deposit, SW Spain. In: Papunen H (ed) Mineral deposits: research and exploration. Balkema, Rotterdam, pp 463–466
Makkonen HV (1996) 1.9 Ga tholeiitic magmatism and related Ni–Cu deposition in the Juva area, SE Finland. Bull Geol Surv Finl 386:101
Marcoux E, Pascual E, Onezime J (2002) Hydrothermalisme ante-Hercynien en Sud-Iberie: apport de la geochimie isotopique du plomb. Compte Rendu Academie Sciences Paris Geosciences 334:259–265
Martín Estévez JR, Ortega L, Lunar R, García Palomero F (2000) Características texturales y geoquímicas de la pirita en la mineralización intramagmática de Ni-Cu-PGE de Aguablanca (Badajoz). Cuad Lab Xeol Laxe 25:107–110
Mateus A, Jesus AP, Oliveira V, Gonçalves MA, Rosa C (2001) Vanadiferous iron–titanium ores in Gabbroic Series of the Beja Igneous Complex (Odivelas, Portugal): remarks on their possible economic interest. Estud Notas Trab Inst Geol Min 43:3–16
Mathez EA (1989) Interactions involving fluids in the Stillwater and Bushveld complexes: observations from the rocks. In: Whitney JA, Naldrett AJ (eds) Ore deposition associated with magmas. Rev Econ Geol 4:167–180
Mathez EA, Peach CL (1989) The geochemistry of the platinum-group elements in mafic and ultramafic rocks. In: Withney JA, Naldrett AJ (eds) Ore deposition associated with magmas. Rev Econ Geol 4:33–44
Matthai SK, Henley RW, Bacigalupo-Rose S, Binns RA, Andrew AS, Carr AR, French DH, McAndrew J, Kavanagh ME (1995) Intrusion related, high temperature gold-quartz veining in the Cosmopolitan Howley metasedimentary rock-hosted gold deposit, N Territory, Australia. Econ Geol 90:1012–1045
McDonough WF, Frey FA (1989) REE in upper mantle rocks. In: Lipin B, McKay GR (eds) Geochemistry and mineralogy of rare earth elements. Rev Miner 21:99–145
McDonough WF, Sun SS (1995) The composition of the earth. Chem Geol 120:223–253
Metcalfe P, McClaren M (2003) The Pacific nickel complex: profile of an environment for magmatic Ni-Cu deposits in a transpressive continental margin setting. In: GAC-MAC Annual Meeting, Vancouver 2003, session SS14
Middlemost EAK (1985) Magmas and magmatic rocks. Longman, London, p 266
Montero P, Salman K, Bea F, Azor A, Exposito I, Lodeiro F, Martinez Poyatos D, Simancas F (2000) New data on the geochronology of the Ossa Morena Zone, Iberian Massif. In: Variscan-Appalachian dynamics: the building of the Upper Paleozoic basement. Galicia 2000, A Coruña, Spain

Nägler T (1990) Sm–Nd, Rb–Sr and common lead isotope geochemistry on fine-grained sediments of the Iberian Massif. Ph.D. thesis, Swiss Federal Institute Technology Zurich, 139 pp. Swiss Federal Institute Technology, Zurich, p 139

Naldrett AJ (1989) Magmatic sulfide deposits. Oxford University Press, London, UK, p 186

Naldrett AJ (1992) A model for the Ni–Cu–PGE ores of the Noril'sk region and the application to other areas of flood basalt. Econ Geol 87:1945–1962

Naldrett AJ (1999) World class Ni–Cu–PGE deposits: key factors in their genesis. Miner Depos 34:227–240

Naldrett AJ (2004) Magmatic sulfide deposits: geology, geochemistry and exploration. Springer, Berlin Heidelberg New York, p 727

Nimis P (1999) Clinopyroxene geobarometry of magmatic rocks: part 2: structural geobarometers for basic to acid, tholeiitic and mildly alkaline magmatic systems. Contrib Mineral Petrol 135:62–74

Ortega L, Moreno T, Lunar R, Prichard H, Sierra J, Bomati O, Fisher P, Garcia Palomero F (1999) Minerales del grupo del platino y fases asociadas en el depósito de Ni–Cu–(EGP) de Aguablanca, SW España. Geogaceta 25:155–158

Ortega L, Lunar R, Garcia Palomero F, Martin Estevez JR (2000) Evidencias de fraccionamiento en el yacimiento intramagmático de Ni–Cu–EGP de Aguablanca (Badajoz). Cuad Lab Xeol Laxe 25:111–114

Ortega L, Lunar R, Garcia Palomero F, Moreno T, Prichard HM (2001) Removilización de minerales del grupo del platino en el yacimiento de Ni–Cu–EGP de Aguablanca (Badajoz). Bol Soc Esp Mineral 24-A:175–176

Ortega L, Lunar R, García Palomero F, Moreno T, Prichard HM (2002) Características geológicas y mineralógicas del yacimiento de Ni–Cu–EGP de Aguablanca (Badajoz). Bol Soc Esp Mineral 25:57–78

Ortega L, Lunar R, Garcia Palomero F, Moreno T, Martin Estevez JR, Prichard HM, Fisher PC (2004) The Aguablanca Ni–Cu–PGE deposit, Southwestern Iberia: magmatic ore-forming processes and retrograde evolution. Can Mineral 42:325–350

Papunen H (2003) Ni–Cu sulfide deposits in mafic–ultramafic orogenic intrusions—examples from the Svecofennian areas, Finland. In: Eliopoulos DG et al (ed) Mineral exploration and sustainable development. Millpress Rotterdam, Rotterdam, pp 551–554

Patiño Douce AE, Castro A, El-Biad M (1997) Thermal evolution and tectonic implications of spinel–cordierite granulites from the Aracena Metamorphic Belt, Southwest Spain. GAC-MAC Annual Meeting, Ottawa, Abstracts volume 22, p A113

Pearce JA (1996) User's guide to basalt discrimination diagrams. In: Wyman DA (ed) Trace element geochemistry of volcanic rocks. Applications for massive sulphide exploration. Geol Assoc Can Short Course 12:79–114

Pin C, Liñan E, Pascual E, Donaire T, Valenzuela E (1999) Late Proterozoic crustal growth in Ossa Morena: Nd isotope and trace element evidence from the Sierra de Cordoba volcanics. XV Reunion Geologia Oeste Peninsular, Abstracts volume, pp 215–218

Piña R, Lunar R, Ortega L, Gervilla F, Alapieti T, Martínez C (2004) Origen de los fragmentos máficos-ultramáficos de la brecha mineralizada del yacimiento de Ni-Cu-EGP de Aguablanca (Badajoz). Macla (Madrid) 2:19–20

Piña R, Gervilla F, Ortega L, Lunar R (2005) Geochemistry and mineralogy of platinum-group elements in the Aguablanca Ni–Cu deposit (SW Spain). In: Törmanen TO, Alapieti T (eds) Platinum group elements—from genesis to beneficiation and environmental impact. 10th International Platinum Symposium, Oulu, Finland, pp 215–218

Pons J (1982) Un modele d'evolution de complexes plutoniques: Gabbros et granitoies de la Sierra Morena Occidentale (Espagne). Doctoral thesis. Laboratoire Geologie Petrologie, Université Paul Sabatier, Tolouse, p 451

Pous J, Muñoz G, Heise W, Melgarejo JC, Quesada C (2004) Electromagnetic imaging of Variscan crustal structures in SW Iberia: the role of interconnected graphite. Earth Planet Sci Lett 217:435–450

Quesada C, Florido P, Gumiel P, Osborne J, Larrea F, Baeza L, Ortega C, Tornos F, Sigüenza J (1987) Mapa Geológico Minero de Extremadura. Junta de Extremadura, Direccion General Industria, Energia y Minas, p 131

Quesada C, Bellido F, Dallmeyer RD, Gil Ibarguchi I, Oliveira TJ, Perez Estaun A, Ribeiro A (1991) Terranes within the Iberian Massif: correlations with West Africa sequences. In: Dallmeyer RD (ed) The West African orogens and Circum-Atlantic correlations. Springer, Berlin Heidelberg New York, pp 267–294

Ripley E (1990) Platinum group element geochemistry of Cu–Ni mineralization in the basal zone of the Babbit Deposit, Duluth Complex, Minnesota. Econ Geol 85:830–841

Ripley EM, Butler BK, Taib NI, Lee I (1993) Hydrothermal alteration in the Babbitt Cu–Ni deposit, Duluth Complex: mineralogy and hydrogen isotope systematics. Econ Geol 88:679–696

Roberts S, Sanderson DJ, Dee S, Gumiel P (1991) Tectonic setting and fluid evolution of auriferous quartz veins from La Codosera area, Western Spain. Econ Geol 86:1012–1022

Rodas M, Luque FJ, Barrenechea JF, Fernandez Caliani JC, Miras A, Fernandez Rodriguez C (2000) Graphite occurrences in the low pressure/high temperature metamorphic belt of the Sierra de Aracena (southern Iberian Massif). Mineral Mag 64:801–814

Rollinson H (1993) Using geochemical data: evaluation, presentation, interpretation. Longman, Essex, p 352

Romeo I, Lunar R, Capote R, Dunning GR, Piña R, Ortega L (2004) Edades de cristalización U–Pb en circones del complejo ígneo de Santa Olalla de Cala: implicaciones en la edad del yacimiento de Ni–Cu-EGP de Aguablanca (Badajoz). Macla (Madrid) 2:29–30

Rudnick RL, Fountain DM (1995) Nature and composition of the continental crust—a lower crustal perspective. Rev Geophys 33:267–309

Ryan B (2000) The Nain Churchill boundary and the Nain plutonic suite: a regional perspective on the geologic setting of the Voisey's Bay Ni–Cu–Co deposit. Econ Geol 95:703–724

Saint Blanquat M, Tikoff B, Teyssier C, Vigneresse JL (1998) Transpressional kinematics and magmatic arcs. In: Holdsworth RE, Strachan RA, Dewey JF (eds) Continental transpressional and transtensional tectonics. Geol Soc Lond Spec Vol 135:327–340

Sanchez Carretero R, Eguiluz L, Pascual E, Carracedo M (1990) Ossa Morena Zone: igneous rocks. In: Martinez E, Dallmeyer RD (eds) Pre-Mesozoic geology of Iberia. Springer, Berlin Heidelberg New York, pp 292–313

Sanderson DJ, Zhang X (1999) Critical stress localization of flow associated with deformation of well-fractured rock masses, with implications for mineral deposits. In: McCaffrey KJW, Lonergan L, Wilkinson JJ (eds) Fractures, fluid flow and mineralization. Geol Soc Lond Spec Vol 155:69–81

Schäfer HJ (1990) Geochronological investigations in the Ossa Morena Zone, SW Spain. Doctoral thesis. Swiss Federal Institute Technology, Zurich, p 153

Shengao Y, Zhaochiong Z, Denghong W, Bailin C, Lixin H, Gang Z (2003) Kalatongke magmatic copper–nickel sulfide deposit. In: Mao J, Goldfarb RJ, Seltmann R, Wang D, Xiao W, Hart CRJ (eds) Tectonic evolution and the metallogeny of the Chinese Altay and Tianshan, pp 131–151

Simancas JF, Carbonell R, Gonzalez Lodeiro F, Perez Estaun A, Juhlin C, Ayarza P, Kashubin A, Azor A, Martínez Poyatos D, Ruiz Almodovar G, Pascual E, Saez R, Expósito I (2003) Crustal structure of the transpressional Variscan orogen of SW Iberia:

SW Iberia deep seismic reflection profile (IBERSEIS). Tectonics 22:1962–1974

Skirrow RG, Sims JP (1999) Genesis and setting of intrusion hosted Ni–Cu mineralization at Las Aguilas, San Luis province, Argentina: implications for exploration of an Ordovician arc. Explor Min Geol 8:1–20

Spiering ED, Rodriguez Pevida L, Castelo JM, Garcia Nieto J, Martinez C (2005) Aguablanca: a new nickel mine in a potential new Ni/Cu and IOCG belt of southern Spain and Portugal. Proceedings Geological Society Nevada. Symposium 2005

Stacey JS, Kramers JD (1975) Approximation of terrestrial lead isotope evolution by a two stage model. Earth Planet Sci Lett 26:207–221

Steiger RH, Jäeger E (1977) Subcommission on geochronology: convention on the use of decay constants in geo- and cosmo-chronology. Earth Planet Sci Lett 36:359–363

Stumpfl EF (1993) Fluids: a prerequisite for platinum metals mineralization. In: Fenoll P, Torres J, Gervilla F (eds) Current research in geology applied to ore deposits, Granada, pp 15–21

Suarez S, Velasco F, Yusta I (2005) Caracterización química y mineralógica de suelos en el yacimiento magmático Ni–Cu de Aguablanca, Badajoz (España). Bol Soc Esp Mineral 3:201–202

Taylor SRM (1995) The geochemical evolution of the continental crust. Rev Geophys 33:241–265

Thompson JFH (1984) Acadian synorogenic mafic intrusions in the Maine Appalachians. Am J Sci 284:462–483

Thompson JFH, Nixon F, Siversten R (1980) The geology of the Vakkerlien nickel prospect, Kvikne, Norway. Bull Geol Soc Finl 52:3–21

Tornos F, Casquet C (2005) A new scenario for related IOCG and Ni–(Cu) mineralisation: the relationship with giant mid-crustal mafic intrusion, Variscan Iberian Massif. Terra Nova 17:286–290

Tornos F, Chiaradia M (2004) Plumbotectonic evolution of the Ossa Morena Zone (Iberian Peninsula): tracing the influence of mantle–crust interaction in ore forming processes. Econ Geol 99:965–985

Tornos F, Velasco F (2002) The Sultana orebody (Ossa Morena Zone, Spain): insights into the evolution of Cu–(Au–Bi) mesothermal mineralization. In: Blundell DJ (ed) GEODE Study Centre, Grenoble, p 17

Tornos F, Casquet C, Galindo C, Canales A, Velasco F (1999) The genesis of the Variscan ultramafic-hosted magmatic Cu–Ni deposit of Aguablanca, SW Spain. In: Stanley et al (eds) Mineral deposits: processes to processing. Balkema, Rotterdam, pp 795–798

Tornos F, Casquet C, Velasco F, Galindo C, Canales A (2000) Las mineralizaciones de Cu–Ni de Aguablanca: un caso inusual de mineralizacion discordante en rocas ultrabásicas (PICG n°427). Temas Geol Min 30:183–191

Tornos F, Casquet C, Galindo C, Velasco F, Canales A (2001) A new style of Ni–Cu mineralization related to magmatic breccia pipes in a transpressional magmatic arc, Aguablanca, Spain. Miner Depos 36:700–706

Tornos F, Casquet C, Galindo C, Velasco F, Canales A (2002a) The Aguablanca Ni–Cu orebody (Ossa Morena Zone, SW Spain): geologic and geochemical features. Bol Soc Esp Mineral 25:99–116

Tornos F, Casquet C, Relvas J, Barriga F, Saez R (2002b) The relationship between ore deposits and oblique tectonics: the SW Iberian Variscan Belt. In: Blundell D, Neubauer F, von Quadt A (eds) The timing and location of major ore deposits: an evolving orogen. Geol Soc Lond Spec Publ 204:179–198

Tornos F, Inverno C, Casquet C, Mateus A, Ortiz G, Oliveira V (2004) The metallogenic evolution of the Ossa Morena Zone. J Iber Geol 30:143–180

Tornos F, Casquet C, Relvas J (2005) The metallogenesis of transpressional orogens: the Variscan of SW Iberia. Ore Geol Rev 27:133–163

Tosdal RM, Nutt CJ (1998) Formation of sedimentary rock-hosted (Carlin-type) Au deposit of the Carlin Trend along an Eocene accommodation zone. Geological Society of America Abstracts with Programs, vol 30

Unrug R, Haranczyk C, Chocyk JM (1999) Eastern Avalonian and Armorican–Cadomian terranes of Central Europe and Caledonian-Variscan evolution of the polydeformed Krakow mobile belt; geological constraints. Tectonophysics 302:133–157

Velasco F (1976) Mineralogía y metalogenia de las skarns de Santa Olalla (Huelva). Doctoral thesis, Universidad del Pais Vasco, Bilbao

Winchester JH, Floyd PA (1977) Geochemical discrimination of different magma series and their differentiation products using immobile elements. Chem Geol 20:325–343

Workman RK, Hart SR (2005) Major and trace element composition of the depleted MORB mantle. Earth Planet Sci Lett 231:53–72